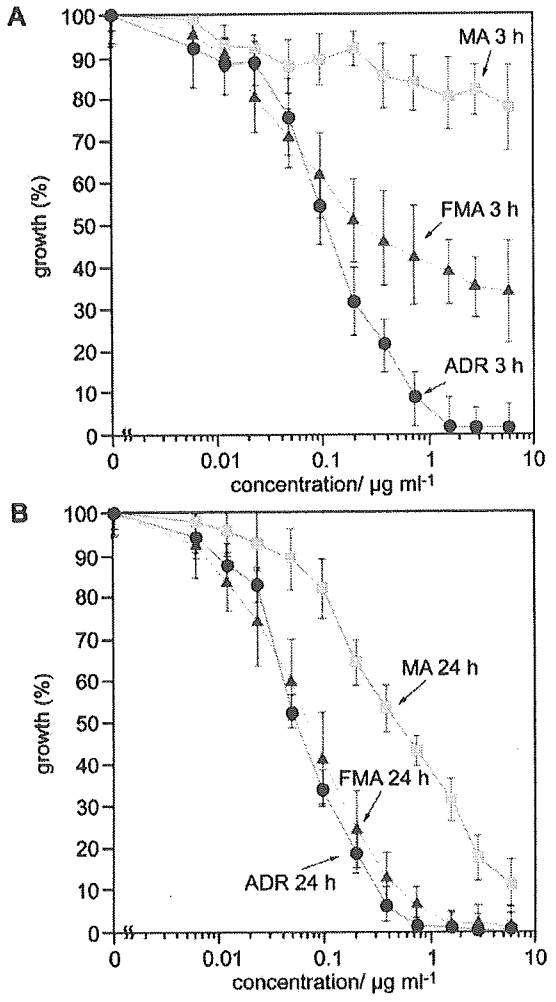

Fig. 4 Correlation between exposure time and cell-growth inhibitory activity of folate-bound pH-sensitive micelles with adriamycin (FMA), folate-unbound pH-sensitive micelles with adriamycin (MA) and free adriamycin (ADR) [3 h exposure (A) and after 24 h incubation (B)].

entering the cell. As summarized in Table 1, it is notable that cytotoxic activity of FMA was as high as 1/1.45 fold with respect to free ADR after 24 h exposure time. Interestingly,

Table 1 Time-dependent growth inhibitory effects of the micelles[a]

Sample	Exposure time/h	IC_{50}[b]/μg ml^{-1} ± SD	Relative index[c]
ADR	3	0.103 ± 0.052	2.19
	24	0.047 ± 0.013	1
FMA	3	0.21 ± 0.104	4.47
	24	0.068 ± 0.039	1.45
MA	3	ND[d]	ND[d]
	24	0.43 ± 0.065	9.15

[a] KB cells were used for the eight independent experiments (n = 8). [b] IC_{50} means the inhibitory concentration of the drugs required for 50% reduction in cell population. The values of the micelles are calculated with the ADR equivalents. [c] Relative index means the ratio between a control and the object for comparison. Here, we evaluated the growth inhibitory effect of the micelle by converting their concentrations with respect to ADR after 24 h incubation as a control. [d] ND denotes 'not determined'.

even though both FMA and MA have equivalent drug contents, cytotoxicity of FMA was 8-fold higher than that of MA in terms of IC_{50} after 24 h incubation. As described above, both FMA and MA are designed to release the loaded drugs only by sensing pH decrease in the cells, and therefore such a great difference in cytotoxicity indicates that a strong FBP-binding effect should be the decisive reason for the enhanced efficacy of the intracellular environment-sensitive polymeric micelles.

Enhanced cellular uptake of the micelles by folate installation

In order to confirm our hypothesis that cellular uptake of the micelles is enhanced by folate installation above, flow cytometric (FCM) analysis was carried out by changing sample exposure time to the cells. Based on the *in vitro* cytotoxicity results, samples (FMA, MA and ADR) were exposed to KB cells for 3 h and 24 h, and increasing fluorescence of the cells was monitored. As shown in Fig. 5,

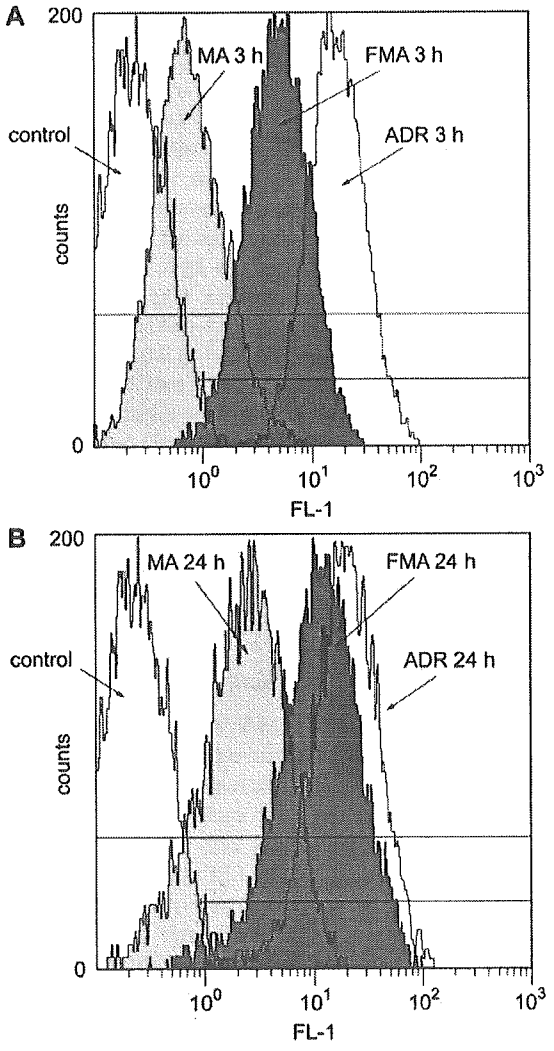

Fig. 5 Flow cytometric histogram profiles of time-dependent change in fluorescence intensity when KB cells were exposed to FMA, MA and ADR for 3 h and 24 h.

the experimental results clearly demonstrated that cellular uptake of FMA drastically increased even with short exposure time (3 h), and the extent was almost similar to that of ADR after 24 h. Although time-dependent increase in fluorescence intensity was also observed in the case of MA, its cellular uptake still remained low in comparison with FMA as well as ADR. Therefore, it is concluded that cellular uptake of the micelles can be significantly accelerated by installing folate on their surfaces, and this conclusion would be one of the most reasonable explanations for the difference between FMA and MA in their cytotoxic activity in spite of equivalent drug loading contents.

Conclusion

This paper describes a novel approach by which a polymeric micelle can be modified as a multifunctional drug carrier for intracellular active drug targeting to elevate the efficacy and safety of the loaded drugs. In order to prepare such micelles, folate was conjugated to the end of shell-forming PEG of amphiphilic PEG–PBLA block copolymers, that self-assembled into a spherical nano-structure in aqueous solutions, while anticancer drugs (ADR) were conjugated through acid-sensitive hydrazone bonds to the side chains of the core-forming PBLA block.

Obtained experimental results demonstrated that this micelle, with both pH sensitivity and receptor selectivity, has a capacity not only to selectively control intracellular environment-sensitive drug release but also to significantly enhance drug delivery efficiency by affecting drug efficacy with short exposure times. For the preparation of folate-bound block copolymers, Fol–PEG–p(Asp-Hyd-ADR), it must be emphasized that our synthetic route ensures the activity of folate for cancer-targeting as well as hydrazide groups for drug-binding. Folate was functionalized at its γ-position to conjugate shell-forming PEG with aldehyde groups at the end of the chain, and this method allows the active folate ligands to conjugate on the surface of the micelles efficiently. SPR analysis showed that the folate-bound micelle was selectively interacting with the immobilized FBP, whereas the folate-unbound micelle seemed unlikely to interact with FBP. Such a characteristic FBP-binding effect of the micelle was also observed against live cells. *In vitro* cytotoxicity assay and FCM analysis clearly indicated that cell growth inhibitory activity of the micelle was enhanced due to enhanced cellular uptake. Consequently, it is concluded that the folate-bound polymeric micelle is an excellent intelligent nano-device for actively delivering drugs inside the cell *via* selective protein-binding affinity, and therefore, this system would provide a safe and effective strategy for new modalities to treat cancers using macromolecular drug carriers that interact with a living body.

Experimental

Materials

β-Benzyl-L-aspartate was from Sigma and α-methoxy-ω-amino poly(ethylene glycol) (PEG; MW = 12 000) was from Nippon Oil & Fats, Japan. PEG was purified using an ion-exchange gel column (CM-Sephadex C-50, Amersham Pharmacia Biotech) prior to the synthesis of the block copolymers. Adriamycin hydrochloride (ADR-HCl) was from Nippon Kayaku, Japan, and its purity was checked by reversed phase liquid chromatograpy (RPLC). Sephadex LH-20 gel was from Amersham Pharmacia Biotech, Sweden.

Tetrahydrofuran (THF), dichloromethane (CH_2Cl_2), *N,N*-dimethyl formamide (DMF), dimethylacetamide (DMAc), anhydrous methanol (MeOH), trifluoroacetic acid (TFA), trifluoroacetic anhydride (TFAA), acetic anhydride (AA), acetonitrile (CH_3CN), methanesulfonyl chloride (CH_3SO_2Cl), triethylamine (TEA) and diethyl ether were purchased from Wako Pure Chemical Industries, Co., Ltd., Japan. THF, DMF, and CH_2Cl_2 were distilled twice following standard procedures. Carbazic acid *tert*-butyl ester (CAt-BE) and potassium carbonate (K_2CO_3) were purchased from Tokyo Kasei Organic Chemicals Co., Ltd., Japan. These chemicals were used without further purification. Folic acid ($C_{19}H_{19}N_7O_6$, MW = 441.4), 4-(diethoxymethyl)benzaldehyde and sodium cyanoborohydride ($NaBH_3CN$) were purchased from Sigma Chemical Co. Ltd., USA. Ethylene oxide (EO) was from Sumitomo Seika Chemicals Co. Ltd., Hyogo, Japan, and dried over calcium hydride followed by the distillation.

Cell lines and animals

A human pharyngeal cancer KB cell line was purchased from Health Science Research Resources Bank, Osaka, Japan. Cells were cultured in Dulbecco's Modified Eagle cell culture Medium (DMEM, Sigma Chemical Co., Inc., USA) containing 10% FBS in a humidified atmosphere with 5% CO_2 at 37 °C.

Devices

Gel permeation chromatography (GPC) measurements were carried out using a TOSOH HLC−8220 equipped with TSKgel columns (G4000PWXL and G3000PWXL). Internal refractive index (RI) and ultraviolet-visible absorption (UV-Vis; 360 nm for folate) detectors were used. DMF with 10 mM LiCl was used as an eluent at a flow rate of 0.8 ml min^{-1} at 40 °C. ^{1}H-NMR spectra were measured with a JEOL EX300 spectrometer (JEOL, Tokyo, Japan). Chemical shifts are reported in ppm relative to the residual protonated solvent resonance.

Synthesis of folate–hydrazide (Fol–Hyd) 10

Folic acid **1** (10 g, 23 mmol) was dissolved in ice-cooled anhydrous THF (100 ml), and an excess amount of TFAA (28 ml, 197 mmol) was slowly added. The mixture gradually turned into a homogeneous solution with a brown color as the reaction proceeded (pyrofolic acid derivatives **2**). After 10 h, ice (10 g) was added to the solution to prepare N^{10}-(trifluoroacetyl)-pyrofolic acid. After precipitation in diethyl ether, the yellow powder was collected by filtration and dried under vacuum. N^{10}-(trifluoroacetyl)pyrofolic acid (5 g, 9.6 mmol) was then dissolved in dry DMF (25 ml), and K_2CO_3 was slowly added at 25 °C. The solution was carefully acidified with 5% aqueous hydrochloric acid. The precipitate

was washed with water and diethyl ether. Pyrofolic acid was dried under vacuum and collected. Pyrofolic acid (500 mg, 1.2 mmol) and CAt-BE (1.6 g, 10 equiv.) were dissolved in 20 ml of dry DMF, and the reaction was allowed to proceed at 40 °C in an argon atmosphere. After 24 h reaction, folate–hydrazide–BOC **3** was precipitated in ether. The precipitate was isolated by centrifugation and then purified by a recycling preparative HPLC (LC918, Japan Analytical Industry Co., Ltd., Tokyo, Japan) and a thin-layer chromatography (TLC, 50 mmol phosphate buffer, pH 7, and acetonitrile = 3 : 1). Subsequently, BOC groups of folate–hydrazide–BOC were removed with TFA, giving Fol–Hyd **4**.

Synthesis of α-4-(diethoxymethyl) benzyl-ω-amine-poly(ethylene glycol) [aceBz-PEG-NH_2] 5

4-(diethoxymethyl)benzaldehyde (15 g, 72 mmol) was dissolved in dry ethanol (300 ml) under argon and the solution was cooled on ice during the addition of sodium borohydride ($NaBH_4$, 3.0 g, 79.3 mmol) as reported elsewhere.[22] The reaction was checked by TLC, eluted with the solution from diethyl ether and hexane (1 : 1). The mixture was put into water (100 ml) and extracted by CH_2Cl_2. The organic solution was washed with anhydrous $MgSO_4$, evaporated, and distillated to give the products. Potassium naphthalene was prepared by adding 3.76 g (96 mmol) of potassium into 300 ml of ice-cold THF in which 11.54 g (90 mmol) of naphthalene was added. After 24 h, unreacted potassium in the solution was removed. Potassium 4-(diethoxymethyl)benzylalkoxide (PDA), that is as an initiator for the polymerization of EO, was then prepared by mixing 4-(diethoxymethyl)benzylalcohol (0.19 g, 0.90 mmol) and potassium naphthalene (0.90 mmol) into dry THF (30 ml) under Ar. After 10 min, 4.5 g (102 mmol) of EO was added to the solution, followed by the reaction at room temperature for 2 days to give aceBz–PEG–OH. Subsequently, α-4-(diethoxymethyl)benzyl-ω-amine-poly(ethylene glycol) [aceBz–PEG–NH_2 **5**] was produced from the prepared aceBz–PEG–OH *via* aceBz–PEG–OSO_2CH_3. aceBz–PEG–OH was mixed with CH_3SO_2Cl (0.62 g, 5.4 mmol) and TEA (0.82 g, 8.1 mmol) in 25 ml of THF. After precipitation in diethyl ether, filtration and dry, aceBz–PEG–OSO_2CH_3 was obtained. Then, 100 ml of 25% ammonia solution was added with respect to 1 g of aceBz–PEG–OSO_2CH_3 and the reaction was allowed to proceed for 2 days. The volume of the solution was concentrated into 200 ml by rotary evaporation and dialyzed against 0.25% ammonia solution, followed by substitution with distilled water and lyophilization to give **5**.

Synthesis of folate–poly(ethylene glycol)–poly(aspartate hydrazone adriamycin) [Fol–PEG–p(Asp–Hyd–ADR) 11]

4-(diethoxymethyl)benzyl–poly(ethylene glycol)–poly(β-benzyl L-aspartate) (aceBz–PEG–PBLA **7**) was synthesized *via* ring-opening polymerization of β-benzyl L-aspartate *N*-carboxyanhydride (BLA–NCA) by using **5** as a macromolecular initiator. Acetylation of the ω-amine group of **7** was carried out with AA to prevent dimerization between aldehyde–benzyl–poly(ethylene glycol)–poly(β-benzyl L-aspartate) (CHO–Bz–PEG–PBLA **8**) block copolymers, which were obtained by deprotecting acetal groups under the acidic condition with the 0.1 N hydrochloric acid aqueous solution. The end-group activated **8** (250 mg) and **4** (50 mg, 10 equiv.) were dissolved in dry DMF and conjugated through an imine formation to give folate–poly(ethylene glycol)–poly(β-benzyl L-aspartate) [Fol–PEG–PBLA **9**]. Because imines are acid-labile, reduction of the bond between **8** and **4** was carried out using $NaBH_3CN$. The extent of folate conjugation on **8** was determined and confirmed by ^{1}H-NMR and GPC measurements, respectively. The benzyl groups of **9** were substituted with hydrazide groups for drug binding by ester–amide exchange (EAE) aminolysis reaction. 500 mg of **9** was dissolved in 10 ml of dry DMF, and anhydrous hydrazine (0.62 mg, MW = 32.05) was added to the solution. The reaction was allowed to proceed at 40 °C for 24 h, followed by the deprotection of remaining benzyl groups with 0.1 N NaOH in water at 25 °C and dialysis against 0.25% ammonia solution. After freeze-drying, 100 mg of the obtained folate–poly(ethylene glycol)–poly(aspartate hydrazide) [Fol–PEG–p(Asp-Hyd) **10**] was dissolved in 50 ml of DMF, and excess amount of ADR–HCl (200 mg, MW = 580), with respect to drug binding hydrazide residues at the side chain of block copolymers, was added. The mixed solution was stirred at room temperature for 24 h while being protected from light and concentrated to a volume of 10 ml under reduced pressure, followed by gel purification using Sephadex LH-20 to completely remove unbound ADR. Applied solution was separated into two fractions and the one eluted first was collected. After precipitation from ether, the final product was evaluated by RPLC to confirm the absence of free ADR. Then, the isolated red folate–poly(ethylene glycol)–poly(aspartate hydrazone adriamycin) block copolymer [Fol–PEG–p(Asp–Hyd–ADR) **11**] was freeze-dried from benzene. Drug loading content in **11** was calculated by cleaving hydrazone linkers in 0.1 N HCl solutions and measuring the released drugs, which were determined by RPLC and UV spectroscopy from the absorbance intensity at 485 nm. Purified **11** was dissolved in DMAc again to prepare micelles by a dialysis method.

Evaluation of folate-binding property of the micelles using surface plasmon resonance (SPR) measurement

To study the interaction between FBP and the folate-bound intracellular pH-sensitive polymeric micelles loading ADR (FMA), surface plasmon resonance (SPR) measurements were performed (BIAcore 3000, Biacore AB, Uppsala, Sweden). The folate unbound polymeric micelles loading ADR (MA) were prepared as control. For the experiments, FBP was immobilized onto the surface of a sensor chip as follows: (1) the device was saturated with PBS buffer (100 mM PBS, pH 7.4); (2) *N*-hydroxysuccinimide (NHS) and 1-ethyl-3-(3-dimethylaminopropyl)-carbodiimide (EDC) were added to the carboxylated dextran-coated sensor chip; (3) FBP dissolved in PBS buffer at a concentration of 200 μg ml^{-1} was injected; and (4) The sensor chip was washed with 1 M ethanolamine aqueous solution to deactivate residual NHS-esters on the surface. The immobilization protocol, which was performed at a flow rate of 10 μl min^{-1}, allowed the binding of 3 ng mm^{-2} of FBP per channel. The binding effects of both FMA and MA to the sensor chip were evaluated by performing SPR

measurements at a flow rate of 10 μl min^{-1} with a concentration of 200 μg ml^{-1}. The micelles were allowed to interact with FBP for 30 min. All samples were tested on newly immobilized FBP.

In vitro growth-inhibition assay

In order to verify the FBP-binding effect of the micelle against live cells, *in vitro* growth-inhibition tests were carried out using a human pharyngeal cancer KB cell line. A tetrazolium dye method, called the MTT assay, was used for the test.[29] Cells were exposed to FMA, MA, and ADR for 3 h and 24 h and washed, followed by 24 h post-incubation. Live cells were then counted using a Bio-RAD Microplate Reader 550 (Bio-Rad Laboratories). Drug concentrations of the micelles were determined based on the amounts of loaded ADR so that IC_{50} values could be compared directly.

Flow cytometric (FCM) analysis

Enhanced cellular uptake of FMA was confirmed using flow cytometry (EPICS XL Flow Cytometry Systems, Beckman Coulter, Inc). Using 12-well culture plates, exponentially growing KB cells were seeded (30 000 cell per well) and pre-incubated for 24 h, followed by coincubation with 10 μg ml^{-1} of FMA, MA, and ADR. After exposure for 3 h and 24 h, the medium was discarded and the cells were washed three times with PBS. Cells were then detached by trypsinization, centrifuged and dispersed again in PBS for the measurements. Data were acquired and processed with the accompanying software (EXPO 32).

Acknowledgements

This research was supported by a Grant-in-Aid for Scientific Research from the Ministry of Education, Culture, Sports, Science and Technology (MEXT), Japan, and by Core Research for Evolutional Science and Technology (CREST), Japan Science and Technology Corporation (JST).

References

1 N. Nishiyama, S. Okazaki, H. Cabral, M. Miyamoto, Y. Kato, Y. Sugiyama, K. Nishio, Y. Matsumura and K. Kataoka, *Cancer Res.*, 2003, **63**, 8977.
2 M. L. Adams, A. Lavasanifar and G. Kwon, *J. Pharm. Sci.*, 2003, **92**, 1343.
3 J. Kopecek, P. Kopeckova, T. Minko, Z. R. Lu and C. M. Peterson, *J. Controlled Release*, 2001, **74**, 147.
4 Y. Takakura and M. Hashida, *Pharm. Res.*, 1996, **13**, 820.
5 H. Maeda and Y. Matsumura, *Crit. Rev. Ther. Drug*, 1989, **6**, 193.
6 R. Duncan, *Nat. Rev. Drug. Discov.*, 2003, **2**, 347.
7 D. S. Goldin, C. A. Dahl, K. L. Olsen, L. H. Ostrach and R. D. Klausner, *Science*, 2001, **292**, 443.
8 K. Kataoka, A. Harada and Y. Nagasaki, *Adv. Drug Delivery Rev.*, 2001, **47**, 113.
9 Y. Bae, S. Fukushima, A. Harada and K. Kataoka, *Angew. Chem., Int. Ed.*, 2003, **42**, 4640.
10 Y. Bae, N. Nishiyama, S. Fukushima, H. Koyama, M. Yasuhiro and K. Kataoka, *Bioconjugate Chem.*, 2005, **16**, 122.
11 A. T. Jones, M. Gumbleton and R. Duncan, *Adv. Drug Delivery Rev.*, 2003, **55**, 1353.
12 S. D. Weitman, R. H. Lark, L. R. Coney, D. W. Fort, V. Frasca, V. R. Zurawski and B. A. Kamen, *Cancer Res.*, 1992, **52**, 3396.
13 I. G. Campbell, T. A. Jones, W. D. Foulkes and J. Trowsdale, *Cancer Res.*, 1991, **51**, 5329.
14 B. Stella, S. Arpicco, M. T. Peracchia, D. Desmaele, J. Hoebeke, M. Renoir, J. D'angelo, L. Cattel and P. Couvreur, *J. Pharm. Sci.*, 2000, **89**, 1452.
15 R. J. Lee and P. S. Low, *J. Biol. Chem.*, 1994, **269**, 3198.
16 A. C. Antony, *Blood*, 1992, **79**, 2807.
17 A. Gabizon, A. T. Horowitz, D. Goren, D. Tzemach, F. Mandelbaum-Shavit, M. M. Qazen and S. Zalipsky, *Bioconjugate Chem.*, 1999, **10**, 289.
18 S. Wang and P. S. Low, *J. Controlled Release*, 1998, **53**, 39.
19 R. J. Lee, S. Wang and P. S. Low, *Biochim. Biophys. Acta*, 1996, **1312**, 237.
20 H. Elnakat and M. Ratnam, *Adv. Drug Delivery Rev.*, 2004, **56**, 1067.
21 J. Luo, M. D. Smith, D. A. Lantrip, S. Wang and P. L. Fuchs, *J. Am. Chem. Soc.*, 1997, **119**, 10004.
22 Y. Akiyama, Y. Nagasaki and K. Kataoka, *Bioconjugate Chem.*, 2004, **15**, 424.
23 M. Wu, W. Gunning and M. Ratnam, *Cancer Epidemiol. Biomarkers Prev.*, 1999, **8**, 775.
24 H. Ogura, M. Yoshinouchi, T. Kudo, M. Imura, T. Fujiwara and Y. Yabe, *Cell. Mol. Biol.*, 1993, **39**, 463.
25 P. C. Elwood, *J. Biol. Chem.*, 1989, **264**, 14893.
26 A. J. M. D'souza and E. M. Topp, *J. Pharm. Sci.*, 2004, **93**, 1962.
27 K. D. Jensen, A. Nori, M. Tijerina, P. Kopeckova and J. Kopecek, *J. Controlled Release*, 2003, **87**, 89.
28 N. Nishiyama, Y. Kato, Y. Sugiyama and K. Kataoka, *Pharm. Res.*, 2001, **18**, 1035.
29 M. C. Alley, D. A. Scudiero, A. Monks, M. L. Hursey, M. J. Czerwinski, D. L. Fine, B. J. Abbott, J. G. Mayo, R. H. Shoemaker and M. R. Boyd, *Cancer Res.*, 1988, **48**, 589.

DNA Cleavage

A Synthetic Block Copolymer Regulates S1 Nuclease Fragmentation of Supercoiled Plasmid DNA**

*Kensuke Osada, Yuichi Yamasaki, Satoshi Katayose, and Kazunori Kataoka**

The materials chemistry and physics of block copolymer supramolecular assembly continue to receive considerable attention in the construction of higher-ordered architectures with unique morphologies and functions.[1–10] Of particular

[*] Dr. K. Osada, Dr. Y. Yamasaki, Prof. Dr. K. Kataoka
Department of Materials Science and Engineering
Graduate School of Engineering, The University of Tokyo
Hongo 7-3-1, Bunkyo, Tokyo 113-8655 (Japan)
Fax: (+81) 3-5841-7139
E-mail: kataoka@bmw.t.u-tokyo.ac.jp
Dr. S. Katayose[+]
Department of Materials Science and Engineering
Tokyo University of Science
Yamazaki 2641, Noda, Chiba 278 (Japan)
[+] Present address:
Tsukuba Research Laboratories
JSR Corporation
25 Miyukigaoka, Tsukuba, Ibaraki 305-0841 (Japan)

[**] This work was supported by The Special Coordination Funds for Promoting Science and Technology, a Grant-in-Aid for Scientific Research on Priority Area A (Molecular Synchronization for Design of New Materials System) from the Ministry of Education, Culture, Sports, Science, and Technology (MEXT), and the Core Research Program for Evolutional Science and Technology (CREST) from the Japan Science and Technology Corporation (JST). The authors thank D. W. Grainger for critical reading of the manuscript.

Supporting Information for this article is available on the WWW under http://www.angewandte.org or from the author.

  DOI: 10.1002/anie.200500201

interest is the exploitation of the spatial order intrinsic to block copolymers for the amplification or modulation of molecular recognition processes by using integrated multisite interactions as well as a distinct spatial matching. Herein we report an unprecedented finding that DNA supramolecular assembly with the synthetic block copolymer poly(ethylene glycol)-*b*-poly(L-lysine) (PEG-PLL)[6,11–14] modulates supercoiled plasmid DNA into a particular structure. The incorporated DNA within the assembly is cleaved into seven distinct regular fragments by S1 nuclease, an enzyme known to cleave single-stranded DNA. The seven characteristic DNA fragments were of well-defined molecular sizes; in each case these were 10/12, 9/12, 8/12, 6/12, 4/12, 3/12, and 2/12 of the original plasmid length (Figure 1). It is notable that the cleaved sites

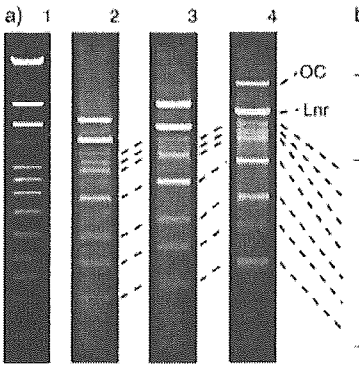

b)

Fragments

Length of the fragment [bp] / Size ratio to the native DNA [%]

no	pBR322 4363 bp	pGL3-Luc 5256 bp	ColE1 6646 bp	ratios in fraction
1	3690 / 84.6	4560 / 84.6	5630 / 84.8	10/12
2	3260 / 75.3	4100 / 76.1	5000 / 75.2	9/12
3	2940 / 67.4	3680 / 68.2	4490 / 67.6	8/12
4	2180 / 50.0	2740 / 50.8	3360 / 50.6	6/12
5	1460 / 33.5	1830 / 34.0	2240 / 33.7	4/12
6	1050 / 24.1	1340 / 24.9	1650 / 24.9	3/12
7	750 / 17.1	910 / 16.8	1090 / 16.4	2/12

Figure 1. Regulated fragmentation of plasmid DNAs complexed with PEG-PLL by the S1 nuclease: a) Gel electrophoresis results. Lane 1: marker DNA; lane 2: pBR322 (4363 bp); lane 3: pGL3-Luc (5256 bp); lane 4: ColE1 (6646 bp). OC = relaxed open circular DNA, Lnr = linearized DNA. b) Length of the obtained fragments and size ratio of them to the native DNA. The size ratio of each fragment from three plasmid DNAs is represented as a fraction in the right-hand column.

are located just outside of protein-coding regions, a fact which simultaneously indicates that the S1 nuclease cuts out genes from DNA.

The block copolymer used in this study comprises a cationic PLL segment, which is the plasmid-binding portion, and a nonionic PEG segment, which forms a hydrophilic and hydrated palisade surrounding the ion-paired complex between PLL and plasmid DNA (see the Supporting Information). This allows to obtain a water-soluble nanoscale assembly (100-nm size) without precipitation. The size-specific plasmid DNA cleavage by S1 nuclease was observed at an acidic pH value of 4.9 for the complex, particularly in a unit molar ratio (amino group/phosphate) of 1.0. As seen in lane 2 of Figure 1a, pBR322 DNA is cut into seven distinct fragments (as listed in Figure 1b). This regular fragmentation was not specific only for pBR322 but seems common for other plasmids. Surprisingly, the other plasmids, pGL3-Luc and ColE1, when complexed with PEG-PLL, were also cut into seven fragments of the same fractions when measured against each original plasmid (Figure 1a, lanes 3 and 4, and Figure 1b). The consistency of the fragmentation results clearly indicates the systematic cleavage of plasmid DNA at well-defined intervals. It should be noted that this regular cleavage of plasmid DNA complexed with PEG-PLL is only observed for the supercoiled DNA form. Relaxed open circular DNA, prepared by treatment with topoisomerase I, also formed stable complexes with PEG-PLL but exhibited no sensitivity to S1 nuclease (data not shown). Additionally, a complex with linear plasmid DNA, prepared by treatment with a restriction enzyme (EcoRI) having a unique recognition site on the plasmid, was smoothly degraded to oligo-DNA pieces in a nonspecific manner (data not shown). The observed differences in S1 nuclease sensitivity to plasmid isomer constructs suggest that topological features of the block copolymer–DNA supramolecular complex influence the enzymatic fragmentation process.

Polyion complex formation between DNA and cationic compounds is known to induce a coil–globule transition, thereby resulting in condensed complexes with ordered morphologies, mainly in toroidal or rod-like forms.[14–18] Consistent with this, charge-neutralizing DNA complexation with PEG-PLL produces a detectable transition from an expanded DNA superhelix into a compact state, as confirmed by static and dynamic light scattering[13] as well as by direct observation with fluorescence microscopy.[18] Although the structural details of the condensed plasmid in this complex have not yet been clarified, significant structural features are probably present in the supercoiled double-stranded DNA upon polyion-induced condensation. Constrained structural order (or regular disorder) in the double-stranded DNA structure might be regularly repeated in this polyion-induced condensation process. This would permit the DNA to adopt particular structures that compensate for the structural constraints accompanying conformation transitions during complexation. Consequently, these specific disordered sites in the condensed DNA strands may preferentially promote S1 nuclease attack, thereby resulting in the observed regular DNA fragmentation.

Supercoiled DNA associated with poly(L-lysine) homopolymer with degrees of polymerization (DP) of 19 and 260 exhibited only nonspecific S1 nuclease degradation without any ordered cleavage, as shown by a smeared electrophoresis gel stain (data not shown). This indicates that polyion complexation alone is not sufficient and that the PEG segment in the block copolymer plays a crucial role in regulating the nuclease sensitivity in addition to promoting the complex solution stability. Inter- or intramolecular steric repulsion of hydrated PEG segments may contribute to the modulated structure of plasmid DNA.

The sensitivity of single-strand-cleavage endonucleases like S1 nuclease against naked plasmid DNAs has been investigated since the 1980s.[19–22] The naked DNAs are first nicked and then linearized. The cleavage sites are cruciform loops, which are adopted by short inverted repeat (palindrome) sequences in the topologically stressed double helix.

Formation of the hairpin-loop structure relieves the topological strain in double-stranded circular DNA molecules. These inverted repeats, separated by nonrepetitious sections of DNA, are specifically cleaved by single-strand-specific nucleases at the center of each hairpin loop. Torsional stress of negative supercoiling of plasmid DNA occasionally induces a kink in the DNA strand with an acute angle. The high susceptibility of palindrome sequences to S1 nuclease digestion led us to assume that the regular fragmentation seen here in the system with the PEG-PLL/plasmid DNA (pDNA) complex might be a result of selective digestion at the cruciform loop regularly induced in the condensed DNA strands. To get an insight into this assumed mechanism, inverted repeats larger than five continuous sequences are picked up from three plasmids (pBR322, pGL3-Luc, and ColE1) by using computer analysis.[23] Neighboring smaller palindromes separated by one or two nonrepetitious sections of DNA were also taken into consideration. It is to be expected that hairpin stability will be directly proportional to stem length but inversely proportional to loop length. The inverted sequences were marked from four to one according to the hairpin stability, as summarized in Figure 2a as a function of base number. Obviously, there are quite a few palindrome sequences. Denaturation of the DNA double strand is necessary for transformation from the normal interstrand base pairing to the intrastrand base pairing of the cruciform structure. The binding energy of the A–T (adenine–thymine) pair is lower than that of the G–C (guanine–cytosine) pair, because two hydrogen bonds are contributing to the pairing between A and T while three contribute between G and C. Thus, the composition of A–T pairs within the palindrome sequences was also examined (Figure 2b). Refinement according to palindrome size and A–T composition allowed the extraction of several sites as candidates for S1 nuclease recognition; these are indicated as dotted lines in Figure 2a and b and as slashes in the pDNA maps (Figure 2d). By use of these refined sites, combinations satisfying the regular fragments were surveyed by consideration of fragment lengths, since two sites on the circular plasmid DNA must be cleaved (for example, 3/12+9/12 = 12/12). Consequently, combinations of cleavage sites yielding the seven DNA sizes were acquired for all three plasmid DNAs

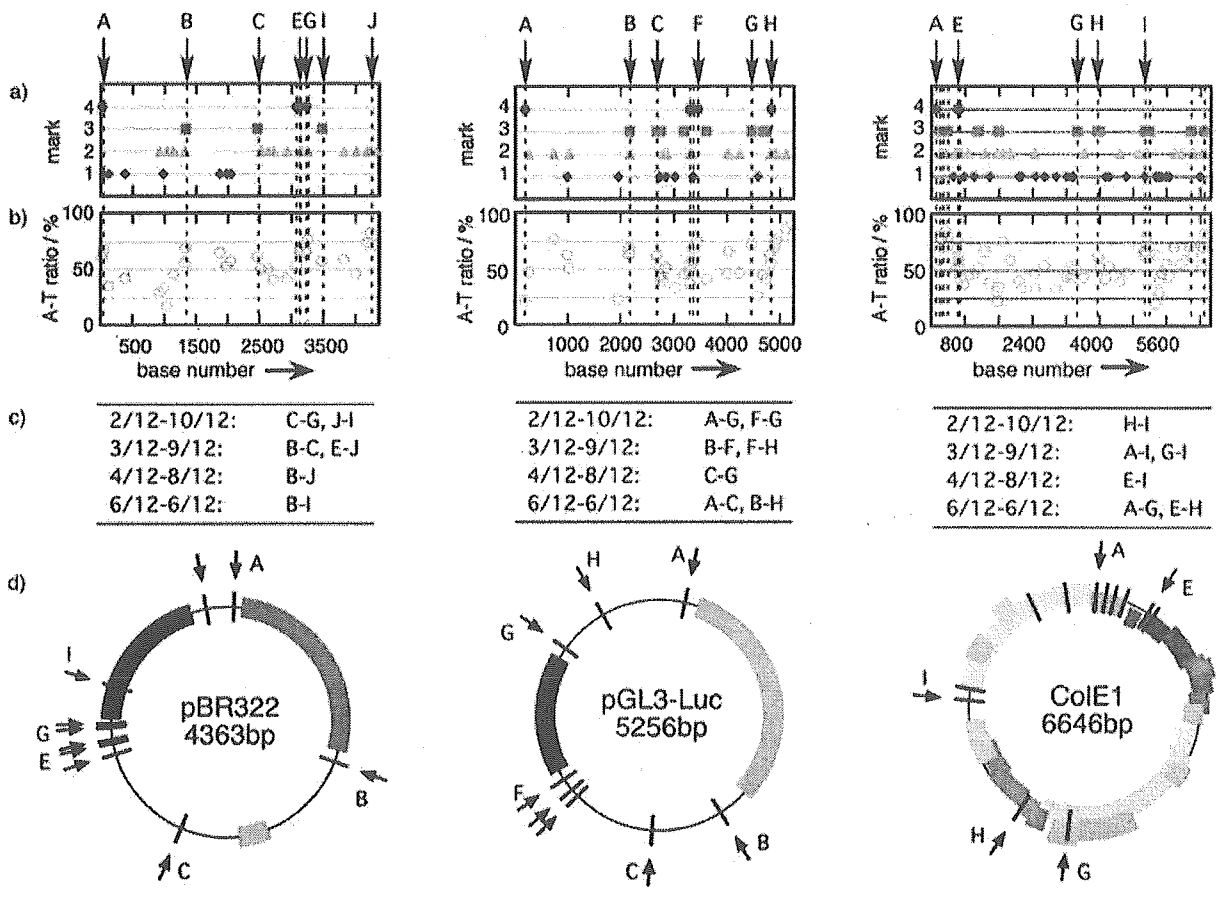

Figure 2. Palindrome maps and protein codes of the three plasmid DNAs pBR322 (left), pGL3-Luc (middle), and ColE1 (right). a) Cruciform stability by the size of inverted repeats. Higher mark numbers indicate higher cruciform stability. b) Percentage A–T composition in the considered palindrome sequences as a function of base number in the plasmid DNAs. Here, base 1 was defined as the recognition site of the EcoR1 restriction enzyme. The dotted lines in panels (a) and (b) indicate refined digestion sites as evaluated from the panels. The combinations of cleavage sites that satisfy the seven-piece fragmentation pattern are summarized in (c). Those evaluated cleavage sites are shown as arrows with capital letters in panels (a) and (d); in addition, correlation between the protein-coding regions and proposed cleavage sites is shown in (d).

(listed in Figure 2c) and those sites are indicated as arrows in Figure 2a and d. The regular fragmentation can be explained by assuming that the cruciform structures regularly induced in the DNA by complexation with the PEG-PLL block copolymer are digested by the single-strand-recognition endonuclease.

Obviously, development of the extruded cruciform structure requires definite stress. The cruciform formation in the naked pDNA is known to be driven by the torsional stress of negative supercoiling.[22] In the complex of pDNA with PEG-PLL, the stress of condensation by the polycation further amplified the torsional stress of the supercoiled conformation, so that the cruciform may be developed in multiple sites. It should be noted that the charge ratio of 1.0 is indeed a critical point in the pDNA transition from extended state to condensed state. The ethidium bromide exclusion assay showed an abrupt decrease in the relative fluorescence, which indicates condensation of DNA molecules, at a charge ratio range of around 1.0 (see the Supporting Information). Additionally, the transition of DNA shape is confirmed by direct observation with atomic force microscopy (Figure 3). Apparently, complex shapes at the charge ratio of 1.0 comprise preferentially condensed rod and toroid conformations.

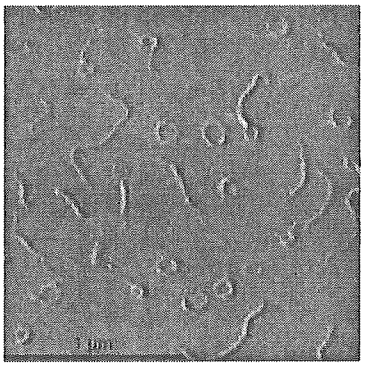

Figure 3. AFM image of plasmid DNA (pGL3-Luc) complexed with the PEG-PLL block copolymer at a charge ratio of 1.0. The image was taken in the amplitude mode for the complex after equilibration in solution for 24 hours. A scale bar is included in the figure.

Furthermore, the potential cleavage site (palindrome site) and protein-coding region have a very interesting correlation, in that the former is located just outside of the latter, as can be clearly seen in Figure 2d. It is worth mentioning that this is commonly observed among the three examined plasmids. This correlation is most distinctive in the ColE1 plasmid, which has various protein codes (Figure 2d). The fact that the selected inverted repeats are located just in the gap or at the terminus of various coding regions suggests that the cruciform structure may substantially contribute to the regulation of gene expression[21] and is most likely to be a landmark for DNA-binding proteins. It should be noted that hypersensitivity of structured DNA to S1 nuclease has been observed in regions of transcriptionally active genes in chromatin.[24] DNA breakage by S1 nuclease is observed in apoptotic cells[25] and also more in mitotic chromosomes than chromosomes in interphase cells.[26] This may be a reflection of the differences of stress under such circumstances. The cruciform structural motifs must be to regulate the binding of proteins, nucleases, promoters, or transcription factors; the full function remains to be determined. Yet, the potential for designing synthetic polymer constructs that reliably alter or mimic these supramolecular structures or for imparting new features of molecular recognition by using the materials of unconventional biopolymer complexes, as demonstrated here, is exciting.

In conclusion, we have demonstrated that the size-specific cleavage of plasmid DNA by S1 nuclease can be mediated by condensed complexes of plasmids with synthetic block copolymers without any sequence-specific binding. The recognition site is probably the cruciform structure induced by DNA complexation with the block copolymer. This means that DNA inherently retains sequences that can transform its secondary structure by certain stimuli and the synthetic polymer reveals the functional structure by complexation. The observed unique sensitivity of PEG-PLL/pDNA complexes to S1 nuclease should provide an insight into the mechanisms of endogenous protein-induced modification of DNA and into the design of artificial restriction enzymes and gene-exploring systems through supramolecular assembly of synthetic macromolecular materials.

Received: January 19, 2005
Published online: May 4, 2005

Keywords: block copolymers · DNA cleavage · hydrolases · molecular recognition · self-assembly

[1] J.-M. Lehn, *Science* **2002**, *295*, 2400–2403.
[2] G. M. Whitesides, B. Grzybowski, *Science* **2002**, *295*, 2418–2421.
[3] J. D. Hartgerink, E. Beniash, S. I. Stupp, *Science* **2001**, *294*, 1684–1688.
[4] D. E. Discher, A. Eisenberg, *Science* **2002**, *297*, 967–973.
[5] S. Jain, F. S. Bates, *Science* **2003**, *300*, 460–464.
[6] A. Harada, K. Kataoka, *Science* **1999**, *283*, 65–67.
[7] J. N. Cha, G. D. Stucky, D. E. Morse, T. J. Deming, *Nature* **2000**, *403*, 289–292.
[8] J. A. Hubbell, *Science* **2003**, *300*, 595–596.
[9] R. Savic, L. Luo, A. Eisenberg, D. Maysinger, *Science* **2003**, *300*, 615–618.
[10] A. V. Kabanov, V. A. Kabanov, *Adv. Drug Delivery Rev.* **1998**, *30*, 49.
[11] S. Katayose, K. Kataoka, *Bioconjugate Chem.* **1997**, *8*, 702–707.
[12] S. Katayose, K. Kataoka, *J. Pharm. Sci.* **1998**, *87*, 160–163.
[13] K. Itaka, K. Yamauchi, A. Harada, K. Nakamura, H. Kawaguchi, K. Kataoka, *Biomaterials* **2003**, *24*, 4495–4506.
[14] K. Miyata, Y. Kakizawa, N. Nishiyama, A. Harada, Y. Yamasaki, H. Koyama, K. Kataoka, *J. Am. Chem. Soc.* **2004**, *126*, 2355–2361.
[15] U. K. Laemmli, *Proc. Natl. Acad. Sci. USA* **1975**, *72*, 4288–4292.
[16] S. M. Mel'nikov, V. G. Sergeyev, K. Yoshikawa, *J. Am. Chem. Soc.* **1995**, *117*, 9951–9956.
[17] J. Rackstraw, A. L. Martin, S. Stolnik, C. J. Roberts, M. C. Garnett, M. C. Davies, S. J. B. Tendler, *Langmuir* **2001**, *17*, 3185–3193.
[18] Y. Yamasaki, S. Katayose, K. Kataoka, K. Yoshikawa, *Macromolecules* **2003**, *36*, 6276–6279.

[19] D. M. J. Lilley, *Nucleic Acids Res.* **1981**, *9*, 1271–1289.
[20] N. Panayotatos, R. D. Wells, *Nature* **1981**, *289*, 466–470.
[21] U. R. Mueller, W. M. Fitch, *Nature* **1982**, *298*, 582–585.
[22] M. Gellert, M. H. O'Dea, K. Mizuuchi, *Proc. Natl. Acad. Sci. USA* **1983**, *80*, 5545–5549.
[23] Palindrome sequence analyses were performed on a Macintosh iBook 400 MHz computer by using the FROG-Mac program (written by N. Miki at Osaka University and available from http://pharma1.med.osaka-u.ac.jp/freeware.html).
[24] A. Larsen, H. Weintraub, *Cell* **1982**, *29*, 609–622.
[25] M. C. Peitsch, C. Mueller, J. Tschopp, *Nucleic Acids Res.* **1993**, *21*, 4206–4209.
[26] G. Juan, W. Pan, Z. Darzynkiewicz, *Exp. Cell Res.* **1996**, *227*, 197–202.

J|A|C|S
COMMUNICATIONS

Published on Web 02/11/2005

PEGylated Polyplex Micelles from Triblock Cationers with Spatially Ordered Layering of Condensed pDNA and Buffering Units for Enhanced Intracellular Gene Delivery

Shigeto Fukushima,[†,§] Kanjiro Miyata,[†,#] Nobuhiro Nishiyama,[*,‡] Naoki Kanayama,[†,#] Yuichi Yamasaki,[†,#] and Kazunori Kataoka[*,†,‡,#]

Department of Materials Science and Engineering, Graduate School of Engineering, The University of Tokyo, 7-3-1 Hongo, Bunkyo-ku, Tokyo 113-8656, Japan, Center for Disease Biology and Integrative Medicine, Graduate School of Medicine, The University of Tokyo, Tokyo 113-0033, Japan, Nippon Kayaku Co., Ltd., and CREST, Japan Science and Technology Agency, Japan

Received September 29, 2004; E-mail: nishiyama@bmw.t.u-tokyo.ac.jp; kataoka@bmw.t.u-tokyo.ac.jp

Successful in vivo gene therapy relies on the development of efficient gene vectors. Especially, the synthetic vectors based on cationic polymers have been attracting much attention because of their safety for clinical application and the variety of their chemical design. Nevertheless, the rational design of synthetic vectors remains to be established. Many previous studies have described that polyplexes formed from polycations with a comparatively low pK_a values, such as polyethylenimine (PEI), show a high transfection activity,[1] which has been explained by the proton sponge effect.[2] However, such polycations have a weak affinity to DNA, resulting in the formation of polyplexes that are easily dissociated under physiological conditions. Also, the buffer capacity of polycations may be hampered by their facilitated protonation due to the zipper effect or the neighboring group effect during the complexation process with DNA.[3] These problems could be modulated by the addition of excess polycations (i.e., increasing the N/P ratios[4]) to form polyplexes with a cationically deviated composition. However, it was recently demonstrated that free polycations in such polyplexes substantially contribute to efficient transfection but also mediate toxic effects. Hence, polyplex systems useful for in vivo gene delivery are required to achieve efficient transfection under the condition without free polycations.[5] Also, the gene delivery systems need to be equipped with high stability and biocompatibility. Here, A−B−C type triblock copolymers consisting of three distinctive functional segments were newly designed for constructing gene delivery systems which might not require free polycations to achieve enhanced gene expression but might provide a high stability and biocompatibility. In the present design of triblock copolymers, poly(ethylene glycol) (PEG) was used as the biocompatible A-segment, poly[(3-morpholinopropyl) aspartamide] (PMPA) was used as the low-pK_a B-segment with a buffering capacity, and poly(L-lysine) (PLL) was used as the high-pK_a C-segment to condense the DNA (Figure 1).

The triblock copolymer, PEG−PMPA−PLL, was synthesized by the successive ring-opening polymerization of the *N*-carboxyanhydrides (NCAs) of β-benzyl-L-aspartate (BLA) and ϵ-(benzyloxycarbonyl)-L-lysine (Lys(Z)), initiated by the $-NH_2$ group of α-methoxy-ω-amino PEG (MW 12 000), followed by the aminolysis of the benzyl ester of PBLA using 4-(3-aminopropyl)morpholine and the deprotection of the Z groups of PLL(Z).[6] The triblock copolymer was confirmed to have a narrow molecular weight distribution (M_w/M_n = 1.18), and the number of repeating units of

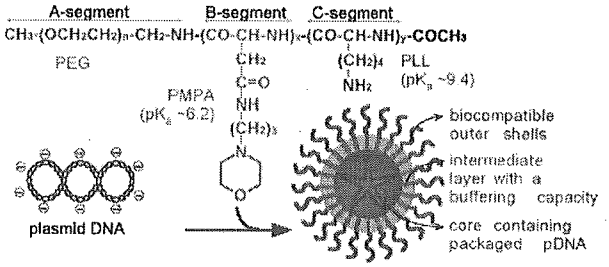

Figure 1. Chemical structure of PEG−PMPA−PLL triblock copolymers and schematic illustration of the hypothesized three-layered polyplex micelles with spatially regulated structure.

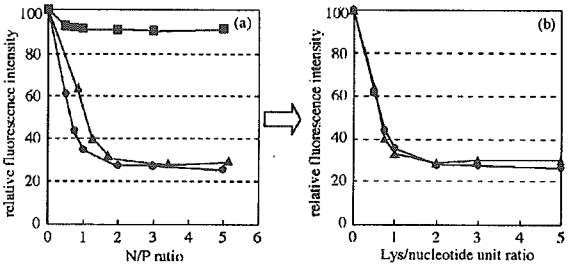

Figure 2. Interaction of PEG−PLL (circle), PEG−PMPA (square), and PEG−PMPA−PLL (triangle) copolymers with pDNA in 10 mM PBS (pH 7.4) + 150 mM NaCl, evaluated by dye exclusion assay. (a) In this figure, the *X*-axis represents the N/P ratio, where N stands for the total of MPA and Lys units. (b) In this figure, the *X* axis represents the Lys/nucleotide unit ratio.

PMPA and PLL was calculated to be 36 and 50, respectively, from the ^{1}H NMR. Diblock copolymers, PEG−PLL with 48 PLL units and PEG−PMPA with 39 PMPA units, were used as comparative samples in this study. The formation of polyplex micelles from these block cationers was confirmed by a gel retardation assay (Figure S4, Supporting Information).[6] Also, the interaction between the di- or triblock copolymers and plasmid DNA (pDNA) was evaluated by an ethidium bromide (EtBr) exclusion assay (Figure 2a). In the case of PEG−PLL (pK_a 9.4), the fluorescence intensity was decreased to 20% of that of the naked pDNA at the N/P ratio of 2. In contrast, the system of PEG−PMPA, having a cationic segment with a lower pK_a value (pK_a 6.2), maintained relatively high fluorescence (>90%) over a wide range of N/P ratios, suggesting that PEG−PMPA lacks the capacity to condense pDNA to a level detectable by this assay. On the other hand, PEG−PMPA−PLL exhibited an 80% decrease in fluorescence at the N/P ratio of 3. Interestingly, the fluorescence profile of PEG−PMPA−

† Graduate School of Engineering, The University of Tokyo.
‡ Graduate School of Medicine, The University of Tokyo.
§ Nippon Kayaku Co., Ltd.
# CREST, Japan Science and Technology Agency.

10.1021/ja0440506 CCC: $30.25

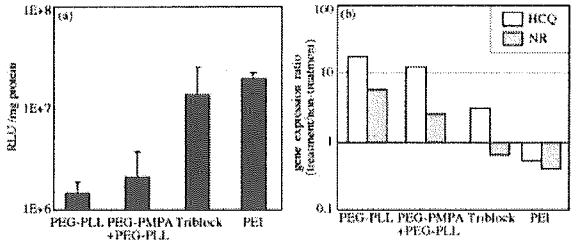

Figure 3. In vitro transfection of luciferase gene to HeLa cells by polyplex micelles from di- or triblock copolymers. HeLa cells were incubated with each micelle in the medium containing 10% serum for 24 h, followed by an additional 24 h incubation without the micelles. (a) The polyplex micelles were prepared at a Lys/nucleotide ratio of 2, and the PEI/pDNA was prepared at the corresponding N/P ratio to the PEG−PMPA−PLL/pDNA. (b) The effects of HCQ and NR on the TE of the polyplexes were evaluated. The PEI polyplex was prepared at the N/P ratio of 10.

PLL/pDNA was almost identical to that of PEG−PLL/pDNA when the N/P ratio was converted to the Lys/nucleotide unit ratio (Figure 2b). Presumably, in the complex of PEG−PMPA−PLL/pDNA, the PLL segment may predominantly contribute to the pDNA condensation. This assumption was confirmed by ^{1}H NMR measurement of PEG−PMPA−PLL/pDNA [Lys/nucleotide ratio = 2 (N/P ratio = 3.4)] in deutereted phosphate-buffered saline (pD 7.4, 150 mM NaCl), in which the chemical shifts assigned to the PLL segment completely disappeared but those assigned to the PMPA segments remained in the spectrum (Figure S6, Supporting Information).[6] This result is consistent with the hypothesis that the PEG−PMPA−PLL/pDNA may form three-layered polyplexes as illustrated in Figure 1. Also, the complete disappearance of PLL peaks from the NMR spectrum suggests that PEG−PMPA−PLL in free form may be minimal in the solution. The size and ζ-potential of the PEG−PMPA−PLL complexes at the Lys/nucleotide ratio of 2 were determined to be 88.7 nm and 7.3 mV, respectively, comparable to those obtained from the PEG−PLL complexes at the N/P ratio of 2 (91.7 nm and 2.1 mV, respectively). The particle size of approximately 100 nm is consistent with the condensed structure of pDNA, and the low absolute value of the ζ-potential suggests the formation of the PEG palisade surrounding the polyplex core.

In vitro transfection efficiency (TE) of the PEG−PMPA−PLL/pDNA at the Lys/nucleotide ratio of 2 was evaluated against HeLa cells. Notably, PEG−PMPA−PLL/pDNA revealed 1 order of magnitude higher TE than PEG-PLL/pDNA (Figure 3a), which was comparable to that of the PEI/pDNA at the corresponding N/P ratio, without showing appreciable cytotoxicity (Figure S9, Supporting Information).[6] On the other hand, the TE of the system composed of (PEG−PMPA + PEG−PLL)/pDNA, where the contents and the repeating units of the PMPA and PLL segments were nearly equal to PEG−PMPA−PLL, was almost the same as that of PEG−PLL. Also, the polyplexes of PEG−PMPA showed no transfection activity over a wide range of N/P ratios (data not shown). These results strongly indicate the importance of aligning in tandem two types of polycations with different pK_a values in a single polymer strand. To study the mechanism of the transfection, the effects of hydroxychloroquine (HCQ) and nigericin (NR) on transfection behavior were investigated. HCQ is known to increase the TE of the polyplexes lacking a buffering capacity, whereas NR could decrease the TE of the polyplexes showing the proton sponge effect.[7] The PEG−PMPA−PLL/pDNA showed less effect of HCQ on enhancing the gene expression compared with the PEG−PLL/pDNA, while it showed an appreciable decrease in the TE in the presence of NR (Figure 3b). Similar trends were also confirmed for 293T cells (Figure S8, Supporting Information). These biological results are consistent with the hypothesis that the enhanced TE of the PEG−PMPA−PLL/pDNA may be attributed to the proton sponge effect. Thus, the buffering capacity of PMPA segment appears to be maintained in the PEG−PMPA−PLL/pDNA under the condition with low Lys/nucleotide ratio. The preferential contribution of the PLL segment to the DNA condensation may ensure the presence of the uncomplexed PMPA segment, even at a comparatively low N/P ratio, to work as a buffering unit.[6]

Nonviral gene vectors used in vivo must have a high stability to be tolerated under harsh conditions in the body. In our previous studies, polyplexes based on PEG−PLL showed a high serum tolerability[8] and prolonged blood circulation.[9] Although the PLL segments form stable polyplexes with pDNA, the transfection activity might be inefficient due to the lack of a proton buffering capacity. In contrast, polycations with a lower pK_a have a buffering capacity for the enhanced transfection but demand a high N/P ratio to achieve a high efficacy. Polyplexes formed at a high N/P ratio may not be useful for in vivo transfection due to stability and toxicity concerns.[5] The result reported here led to the novel design of nonviral gene vectors, overcoming the problems of conventional systems based on the proton sponge concept, using the A−B−C type triblock copolymers, PEG−PMPA−PLL (Figure 1). The results are consistent with the hypothesis that PEG−PMPA−PLL might form three-layered polyplex micelles consisting of a core of pDNA/PLL polyion complexes, an intermediate layer of PMPA segments with a buffer capacity, and an outer shell of biocompatible PEG segments. The PEG−PMPA−PLL polyplexes showed a significantly enhanced transfection activity through the buffering capacity of the PMPA segment, while efficiently compacting pDNA by the PLL segment. Importantly, this increased transfection was achieved under the condition where free or loosely associated polycations are assumed to be minimal, facilitating the future utility of this polyplex micelle for in vivo gene delivery.

Acknowledgment. This work was supported by the Core Research for Evolutional Science and Technology (CREST) from the Japan Science and Technology Agency (JST).

Supporting Information Available: Synthetic method and characterization of triblock copolymers as well as additional data on the physicochemical and biological properties of the PEG−PMPA−PLL/pDNA. This material is available free of charge via the Internet at http://pubs.acs.org.

References

(1) (a) Boussif, O.; Lezoualc'h, F.; Zanta, M. A.; Mergny, M. D.; Scherman, D.; Demeneix, B.; Behr, J.-P. *Proc. Natl. Acad. U.S.A.* **1995**, *92*, 7297−7301. (b) Tang, M. X.; Szoka, F. C. *Gene Ther.* **1997**, *4*, 823−832. (c) Midoux, P.; Monsigny, M. *Bioconjugate Chem.* **1999**, *10*, 406−411. (d) Cherng, J.-Y.; Wetering, P.; Talsma, H.; Crommelin, D. J. A.; Hennink, W. E. *Pharm. Res.* **1996**, *13*, 1038−1042.
(2) Behr, J.-P. *Chemia* **1997**, *51*, 34−36.
(3) Kabanov, A. V.; Bronich, T. K.; Kabanov, V. A.; Yu, K.; Eisenberg, A. *Macromolecules* **1996**, *29*, 6797−6802.
(4) The ratio of the cationic moiety in polycations to the phosphate in DNA.
(5) Boeckle, S.; Gersdorff, K.; Piepen, S.; Culmsee, C.; Wagner, E.; Ogris, M. *J. Gene Med.* **2004**, *6*, 1102−1111.
(6) See Supporting Information.
(7) Lim, Y.-B.; Kim, S.-M.; Suh, H.; Park, J.-S. *Bioconjugate Chem.* **2002**, *13*, 952−957.
(8) (a) Itaka, K.; Harada, A.; Nakamura, K.; Kawaguchi, H.; Kataoka, K. *Biomacromolecules* **2002**, *3*, 841−845. (b) Itaka, K.; Yamauchi, K.; Harada, A.; Nakamura, K.; Kawaguchi, H.; Kataoka, K. *Biomaterials* **2003**, *24*, 4495−4506.
(9) Harada-Shiba, M.; Yamauchi, K.; Harada, A.; Takamisawa, I.; Shimokado, K.; Kataoka, K. *Gene Ther.* **2002**, *9*, 407−414.

JA0440506

Articles

Stabilization of Lysozyme-Incorporated Polyion Complex Micelles by the ω-End Derivatization of Poly(ethylene glycol)−Poly(α,β-aspartic acid) Block Copolymers with Hydrophobic Groups

Xiaofei Yuan,[†] Atsushi Harada,[‡] Yuichi Yamasaki,[†] and Kazunori Kataoka*[,†,§]

Department of Materials Engineering, Graduate School of Engineering, The University of Tokyo, 7-3-1 Hongo, Bunkyo-ku, Tokyo 113-8656, Japan, Department of Applied Materials Science, Graduate School of Engineering, Osaka Prefecture University, 1-1 Gakuen-cho, Sakai, Osaka 599-8531, Japan, and Center for Disease Biology and Integrative Medicine, Graduate School of Medicine, The University of Tokyo, 7-3-1 Hongo, Bunkyo-ku, Tokyo 113-0033, Japan

Received May 6, 2004. In Final Form: December 23, 2004

To improve the stability of lysozyme-incorporated polyion complex (PIC) micelles in physiological condition, three types of hydrophobic groups, including phenyl (Phe), naphthyl (Nap), and pyrenyl (Py) terminal groups, were separately introduced to the ω-end of poly(ethylene glycol)−poly(α,β-aspartic acid) block copolymers (PEG−P(Asp)). The goal was to enhance association forces between the enzyme, lysozyme, and PEG-P(Asp) carriers. Introduction of these hydrophobic groups significantly decreases micellar critical association concentration and increases the micellar tolerability against increasing NaCl concentrations. Particularly, PIC micelles formed from PEG−P(Asp) with Py groups was most stable against increasing NaCl concentrations up to 0.1 M. Significant deviation from a spherical shape for the micelles was also observed for the PEG−P(Asp)−Py system, consistent with an increased association number.

Introduction

Recently, polyion complex (PIC) micelles from charged block copolymers have received growing attention as functional nanomaterials.[1−3] The complexes are formed through Coulombic interactions, not only for pairs of oppositely charged block copolymers or a block copolymer and homopolymer but also for combinations of block copolymers and charged biomacromolecules, including enzymes[4] and DNA.[1b,c,e,f,2a,c,d,3] The latter carriers are useful in pharmaceutical and biochemical fields because entrapped biomacromolecules are protected by the micellar structure and may attain increased stability against various environmental factors, e.g., unfavorable enzyme attack.[5]

Since the discovery of enzyme-incorporated PIC micelles in 1998,[4a] detailed physicochemical characterization of PIC micelles, prepared from chicken egg white lysozyme (a cationic model enzyme) and poly(ethylene glycol)−poly(α,β-aspartic acid) block copolymers (PEG−P(Asp)), has been reported.[4b−e] In brief, this lysozyme-entrapped micelle has acceptable colloidal stability with a narrow size distribution, and the core can behave as a protective nanoreservoir for lysozyme to modulate its stability and activity. For example, the apparent activity of entrapped lysozyme was found to be appreciably higher than that of free lysozyme.[4d,e] Additionally, the capability to on−off regulate the activity of entrapped lysozyme by micellar dissociation and re-formation responding to a salt concentration (ionic strength) of the milieu[4c] or to an external electric field[4e] was also observed. This PEG−P(Asp)/lysozyme micelles was therefore considered to have promise as a biofunctional nanodevice. Nevertheless, its instability at physiological salt concentration remains an obstacle, due to an appreciably weak electrostatic interaction between the P(Asp) segments and basic lysozyme, resulting from a nonhomogeneous charge distribution on the lysozyme surface.

* To whom correspondence should be addressed: Professor Kazunori Kataoka, Department of Materials Engineering, Graduate School of Engineering, The University of Tokyo, 7-3-1 Hongo, Bunkyo-ku, Tokyo 113-8656, Japan. E-mail: kataoka@bmw.t.u-tokyo.ac.jp.

[†] Department of Materials Engineering, Graduate School of Engineering, The University of Tokyo.

[‡] Department of Applied Materials Science, Graduate School of Engineering, Osaka Prefecture University.

[§] Center for Disease Biology and Integrative Medicine, Graduate School of Medicine, The University of Tokyo.

(1) (a) Harada, A.; Kataoka, K. *Macromolecules* **1995**, *28*, 5294. (b) Kataoka, K.; Togawa, H.; Harada, A.; Yasugi, K.; Matsumoto, T.; Katayose, S. *Macromolecules* **1996**, *29*, 8556. (c) Katayose, S.; Kataoka, K. *Bioconjugate Chem.* **1997**, *8*, 702. (d) Harada, A.; Kataoka, K. *Science* **1999**, *283*, 65. (e) Kataoka, K. Harada, A.; Nagasaki, Y. *Adv. Drug Delivery Rev.* **2001**, *47*, 113. (f) Harada-Shiba, M.; Yamauchi, K.; Harada, A.; Takamisawa, I.; Shimokado, K.; Kataoka, K. *Gene Ther.* **2002**, *9*, 407.

(2) (a) Kabanov, A. V.; Vinogradov, S. V.; Suzdaltseva, Y. G.; Alakhov, V. Y. *Bioconjugate Chem.* **1995**, *6*, 639. (b) Kabanov, A. V.; Bronich, T. K.; Kabanov, V. A.; Yu, K.; Eisenberg, A. *Macromolecules* **1996**, *29*, 6797. (c) Kabanov, A. V.; Kabanov, V. A. *Adv. Drug Delivery Rev.* **1998**, *30*, 49. (d) Roy, S.; Zhang, K.; Roth, T.; Vinogradov, S.; Kao, R. S.; Kabanov, A. *Nat. Biotechnol.* **1999**, *17*, 476.

(3) (a) Wolfrert, M. A.; Schacht, E. H.; Toncheva, V.; Ulbrich, K.; Nazarova, O.; Seymour, L. W. *Human Gene Ther.* **1996**, *7*, 2123. (b) Dash, P. R.; Toncheva, V.; Schacht, E.; Seymour, L. W. *J. Controlled Release* **1997**, *48*, 269.

(4) (a) Harada, A.; Kataoka, K. *Macromolecules* **1998**, *31*, 288. (b) Harada, A.; Kataoka, K. *Langmuir* **1999**, *15*, 4208. (c) Harada, A.; Kataoka, K. *J. Am. Chem. Soc.* **1999**, *121*, 9241. (d) Harada, A.; Kataoka, K. *J. Controlled Release* **2001**, *72*, 85. (e) Harada, A.; Kataoka, K. *J. Am. Chem. Soc.* **2003**, *125*, 15306. (f) Jatsuranpinyo, M.; Harada, A.; Yuan, X.-F.; Kataoka, K. *Bioconjugate Chem.* **2004**, *15*, 344.

(5) (a) Katayose, S.; Kataoka, K. *J. Pharm. Sci.* **1998**, *87*, 160. (b) Harada, A.; Kataoka, K. *Eur. J. Pharm. Sci.* **2001**, *13*, 35.

10.1021/la0488811 CCC: $30.25
Published on Web 02/12/2005

Chart 1

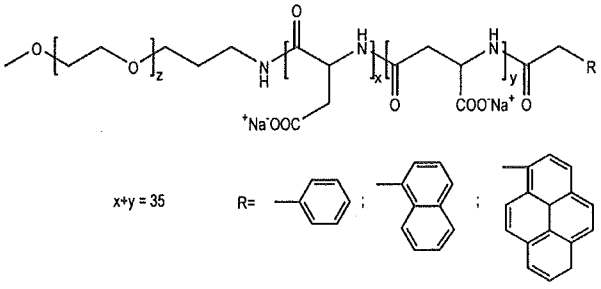

In this study, to solve this micellar instability challenge at increased salt concentrations, three aromatic groups—phenyl, naphthyl, and pyrenyl—were separately introduced to ω-ends of the P(Asp) segment in PEG–P(Asp). Notably, both stability and shape of the PEG–P(Asp)/lysozyme micelles significantly depend on the structure of the end-functional groups. Especially, the pyrenyl terminal groups exhibited the most stabilizing contribution to micelles with increasing media ionic strength.

Experimental Section

Materials. Poly(ethylene glycol)–poly(β-benzyl-L-aspartate) block copolymer (PEG–PBLA, PEG molecular weight is 12 000 g/mol, and degree of polymerization for PBLA is 35, M_w/M_n = 1.06) was synthesized as previously reported.[6] Thionyl chloride, 1-naphthaleneacetic acid, and phenylacetyl chloride were purchased from Wako Pure Chemical Industries, Co., Ltd. (Osaka, Japan). 1-Pyreneacetic acid and chicken egg white lysozyme were obtained from Aldrich Co., Ltd. (Milwaukee, WI) and Sigma (St. Louis, MO), respectively. They were all used without further purification.

Synthesis of ω-(1-Pyrenylacetamido)–Poly(ethylene glycol)–Poly(α,β-aspartic acid) Block Copolymers (PEG–P(Asp)–Py). ω-(1-Pyrenylacetamido)–poly(ethylene glycol)–poly(α,β-aspartic acid) block copolymer (PEG–P(Asp)–Py) was obtained by alkali hydrolysis (0.5 M NaOH) of the side chain benzyl groups in the ω-(1-pyrenylacetamido)–poly(ethylene glycol)–poly(β-benzyl-L-aspartate) block copolymer (PEG–PBLA–Py), prepared first by reaction of 1-pyrenylacetyl chloride with terminal primary amino groups in PEG–PBLA block copolymer (dry argon atmosphere, anhydrous dimethyl formamide (DMF) at 40 °C for 48 h). The molar ratio of 1-pyrenylacetyl chloride to PEG–PBLA was 10:1. The 1-pyrenylacetyl chloride was synthesized by the reaction of 1-pyrenylacetic acid with thionyl chloride at 80 °C for 24 h. After removal of excess thionyl chloride under vacuum, 1-pyrenylacetyl chloride was obtained and immediately used because of its high reactivity. ^{1}H NMR measurement (270 MHz) was performed in D_2O mixed with 30% DMSO-d_6 (to improve solubility of pyrenyl (Py) groups) at 80 °C to calculate the conversion of the terminal primary amino groups in PEG–PBLA to 1-pyrenylacetyl groups (ϕ_{Py}) from the peak intensity ratio of the introduced 1-pyrenylacetyl protons ($COCH_2C_{16}H_9$: δ = 8.2 ppm) to the methylene protons of PEG (OCH_2CH_2: δ = 3.7 ppm). ϕ_{Py} was calculated to be 90%. The ω-(phenylacetamido)–poly(ethylene glycol)–poly(α,β-aspartic acid) block copolymer (PEG–P(Asp)–Phe) and ω-(1-naphthylacetamido)–poly(ethylene glycol)–poly(α,β-aspartic acid) block copolymer (PEG–P(Asp)–Nap) were also prepared using a similar method. ϕ_{Nap} ($COCH_2C_{10}H_7$: δ = 7.6 and 7.9 ppm) and ϕ_{Phe} ($COCH_2C_6H_5$: δ = 7.2 ppm) were calculated to be 82% and 81%, respectively. The structures of these synthesized polymers are illustrated in Chart 1.

Preparation of Polyion Complex (PIC) Micelles. PIC micelles were prepared by a previously reported procedure.[4a,b] Briefly, the synthesized block copolymers, including PEG–P(Asp), PEG–P(Asp)–Phe, PEG–P(Asp)–Nap, and PEG–(Asp)–Py, and lysozyme were separately dissolved in phosphate buffer solution (PBS, 10 mM, pH 7.4; $Na_2HPO_4 \cdot 12H_2O$, 2.865 g/L; $NaH_2PO_4 \cdot 2H_2O$, 0.312 g/L). After filtration through a 0.1 μm filter, each block copolymer was mixed with lysozyme at the mixing ratio r = 1 (r = [Asp residues in PEG-P(Asp)]/[Lys and Arg residues in lysozyme]) to form the PIC micelles. Here, we abbreviate micelles from PEG–P(Asp), PEG–P(Asp)–Phe, PEG–P(Asp)–Nap, and PEG–(Asp)–Py, as PL, PL–Phe, PL–Nap, and PL–Py micelles, respectively.

Light Scattering Measurements. Dynamic and static light scattering (DLS and SLS) measurements were performed using a DLS-7000 instrument (Otsuka Electronic Co., Ltd., Japan). Vertically polarized light of 488 nm wavelength from an Ar ion laser (75 mW) was used as the incident beam.

In DLS measurement, the general formula for the photoelectron-count time correlation function has the form expressed by eqs 1 and 2[7]

$$g^{(2)}(\tau) = 1 + \beta|g^{(1)}(\tau)|^2 \quad (1)$$

$$g^{(1)}(\tau) = \int G(\Gamma) \exp(-\Gamma\tau)\, d\Gamma \quad (2)$$

where $g^{(2)}(\tau)$ is the normalized second-order correlation function, β is a parameter of the optical system constant, $g^{(1)}(\tau)$ is the normalized first-order correlation function, τ is the delay time, Γ is the characteristic line width, and $G(\Gamma)$ is a distribution of Γ. When $g^{(1)}(\tau)$ is analyzed using the cumulant method,[8] it can be expressed by

$$g^{(1)}(\tau) = \exp[-\bar{\Gamma}\tau + (\mu_2/2)\tau^2 - (\mu_3/3!)\tau^3 \cdots] \quad (3)$$

yielding a variance, $\mu_2/\bar{\Gamma}^2$, called the polydispersity index[9] (PDI), and the average characteristic line width, $\bar{\Gamma}$, from which the z-averaged diffusion coefficient (D) is obtained from[7]

$$\bar{\Gamma} = Dq^2 \quad (4)$$

$$q = (4\pi n/\lambda) \sin(\theta/2) \quad (5)$$

Here q is the magnitude of the scattering vector and θ is the detection angle. In the diluted concentration region, the corresponding hydrodynamic radius, R_h, can then be calculated using the Stokes–Einstein equation[10]

$$R_h = k_B T/(6\pi\eta D) \quad (6)$$

where k_B is the Boltzmann constant, T is the absolute temperature, and η is the solvent viscosity. The size distribution was estimated from the correlation function profile using the histogram method.[11]

In SLS measurement, the light scattered by a dilute polymer solution is expressed as[12]

$$KC/\Delta R(\theta) = P(\theta)^{-1}/M_{w,app} + 2A_2C \quad (7)$$

$$P(\theta)^{-1} = 1 + q^2R_g^2/3 - \cdots \quad (8)$$

$$K = (4\pi^2n^2(dn/dc)^2)/(N_A\lambda^4) \quad (9)$$

where C is the polymer concentration, $\Delta R(\theta)$ is the difference in the Rayleigh ratio between the solution and solvent, $P(\theta)$ is the

(6) (a) Yokoyama, M.; Inoue, S.; Kataoka, K.; Yui, N.; Sakurai, Y. *Makromol. Chem. Rapid Commun.* **1987**, *8*, 431. (b) Yokoyama, M.; Inoue, S.; Kataoka, K.; Yui, N.; Okano, T.; Sakurai, Y. *Makromol. Chem.* **1989**, *190*, 2041.

(7) Burchard, W. In *Light Scattering: Principles and Development*; Brown, W., Ed.; Clarendon Press: New York, 1996; Chapter 13, p 438.

(8) Koppel, D. E. *J. Chem. Phys.* **1972**, *57*, 4814.

(9) $\mu_2/\bar{\Gamma}^2$ is referred as polydispersity index, which comes from the equation: $\ln[g^{(1)}(\tau)] = -\bar{\Gamma}\tau + (\mu_2/2)\tau^2 \cdots$, obtained from the cumulant method. If micellar size distribution is unimodal, $\ln[g^{(1)}(\tau)] = -\Gamma\tau$, suggesting $\ln[g^{(1)}(\tau)]$ has a linear relation with τ, and $-\Gamma$ is the slop. When the polydispersity index is <0.1 ($\mu_2/\bar{\Gamma}^2 < 0.1$), μ_2 is smaller than $0.1\bar{\Gamma}^2$. In this case, $-\bar{\Gamma}\tau + (\mu_2/2)\tau^2 \cdots$ insignificantly deviates from $-\bar{\Gamma}\tau$, namely, this size distribution can be acceptable as a unimodal one.

(10) Einstein, A. *Ann. Phys.* **1905**, *17*, 549.

(11) Gulari, E.; Tsunashima, Y.; Chu, B. *J. Chem. Phys.* **1979**, *70*, 3965.

(12) Zimm, B. H. *J. Chem. Phys.* **1948**, *16*, 1093.

Table 1. Determined cac Values (mg/mL) for PIC Micelles at Various NaCl Concentrations

micelle	[NaCl], 0 mol/L	[NaCl], 0.05 mol/L	[NaCl], 0.08 mol/L	[NaCl], 0.1 mol/L
PL	0.25	0.46		
PL–Phe	0.13	0.47	0.62	
PL–Nap	0.13	0.21	0.61	
PL–Py	0.027	0.23	0.50	0.62

particle scattering factor, $M_{w,app}$ is the apparent weight average molar mass, R_g^2 is the mean square radius of gyration, A_2 is the second virial coefficient, and N_A is Avogadro's number. The known Rayleigh ratio of benzene was used as a calibration standard. For lysozyme-incorporated PIC micelles, refractive index increments, dn/dc, were calculated from dn/dc values for lysozyme and PEG–P(Asp) block copolymer with or without hydrophobic groups, using a similar method as described in ref 4a.

Calculation of $P(\theta)^{-1}$ and $(qR_g)^2$ Parameters. To estimate $P(\theta)^{-1}$ as a function of $(qR_g)^2$ for PL, PL–Phe, PL–Nap, and PL–Py micelles, $P(\theta)^{-1}$ and $(qR_g)^2$ were separately calculated using SLS results. The R_g was obtained from the Zimm plot, and these values are summarized in Table 2. Parameter q was directly calculated using eq 5 where θ ranged from 40° to 150° with a 10° interval. The $P(\theta)^{-1}$ parameter came from eq 7. But considering the critical association behavior of the micelles, a correction by both critical association concentration (cac) and $\Delta R(\theta)_{cac}$ values was performed as[4b]

$$K(C - \text{cac})/(\Delta R(\theta) - \Delta R(\theta)_{cac}) = P(\theta)^{-1}/M_{w,app} + 2A_2(C - \text{cac}) \quad (10)$$

where $M_{w,app}$ was also obtained from a Zimm plot and is shown in Table 2. When $C - \text{cac} \rightarrow 0$

$$P(\theta)^{-1} = M_{w,app}[K(C - \text{cac})/(\Delta R(\theta) - \Delta R(\theta)_{cac})] \quad (11)$$

Thus, obtained $P(\theta)^{-1}$ and q values at constant angles were used as a pair to make the $P(\theta)^{-1}$ curve plotted against $(qR_g)^2$.

Results and Discussion

I. DLS Measurements for PIC Micelles. DLS measurements revealed a unimodal size distribution for all micelles, and the cumulant diameters were 58 nm (PL micelles), 61 nm (PL–Phe micelles), 81 nm (PL–Nap micelles), and 87 nm (PL–Py micelles), respectively. Figure 1 shows changes in the cumulant diameter with an increase in total concentration for the system (lysozyme + PEG–P(Asp) with or without ω-end-functional groups). The cumulant micelle diameters remained constant regardless of concentration change—and increased in the order PL < PL–Phe < PL–Nap < PL–Py micelles. This trend may correlate with the difference in the micellar hydrophobic association force, which increases with the same order.[13] These constant diameters for each micelle system also suggest that an increasing concentration induces no formation of secondary micellar aggregation, consistent with an assumed core–shell structure for all micelles. Steric repulsion of the exposed PEG corona may effectively ensure a reasonable micellar stability and

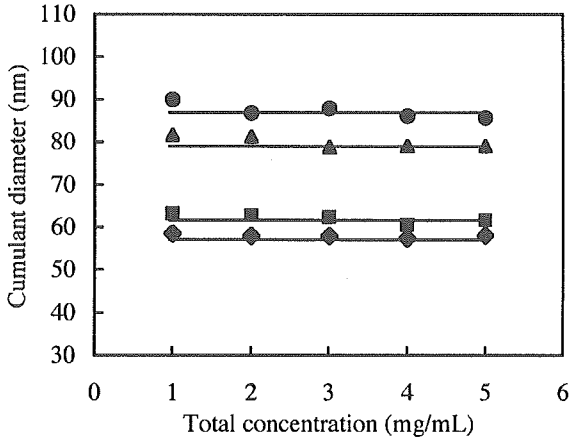

Figure 1. Variations in cumulant diameters with total concentration of the system (lysozyme + PEG–P(Asp) with or without ω-end-functional groups) measured by DLS: detection angle = 90°, temperature = 25 ± 0.2 °C, total concentration = 0.01–5.0 mg/mL; PL micelles (◆), PL–Phe micelles (■), PL–Nap micelles (◆), PL–Py micelles (●).

solubility. The PDI for PL, PL–Phe, and PL–Nap micelles ranged from 0.02 to 0.1, suggesting a unimodal distribution for the micelles. However, the PDI for PL–Py micelles shows slightly higher value (ca. 0.12), discussed in the following section.

II. Micellar Stability in a Dilute Concentration Range. It is well documented in the literatures that the critical association concentration (cac) decreases with an increase in the stability of the micelle state.[14] Thus, the effects of introduced hydrophobic groups on micellar stability may be quantitatively estimated by comparing their cac values.

Detailed determination of cac values uses the Debye plots[15] from SLS data expressed in the form

$$KC/\Delta R(0) = 1/M_{w,app} + 2A_2C \quad (12)$$

The $KC/\Delta R(0)$ curves plotted against C for all micelles are shown in Figure 2. From these curves, the micellar cac values were calculated and are summarized in Table 1 at NaCl = 0 M. Here, the cac was defined as the intersection of two linear components (in lower and higher concentration regions, respectively) in each relation curve.[4a,b] It is apparent that the cac values for PL–Phe, PL–Nap, and PL–Py micelles are lower than that for PL micelles, reflecting an improved micellar stability at NaCl = 0 M due to these introduced terminal hydrophobic groups in P(Asp) segments. Notably, the PL–Py micelles had a significantly lower cac value (0.027 mg/mL) compared with the PL–Phe (0.13 mg/mL) and PL–Nap micelles (0.13 mg/mL), and nearly 1 order of magnitude lower than that for the PL micelles (0.25 mg/mL), suggesting that the PL–Py micelle is the most stable.

Table 2. Characteristics of PIC Micelles Determined from Light Scattering Analysis

micelles	$M_{w,app}$[b] (g/mol)	R_g[b] (nm)	R_h[a] (nm)	R_g/R_h	A_2[b] (mol·mL/g^2)	association no.[c] P(Asp)	association no.[c] lysozyme
PL	2.59×10^6	19.4	29	0.67	2.31×10^{-5}	56	117
PL–Phe	4.49×10^6	27.9	31	0.90	3.02×10^{-5}	96	202
PL–Nap	11.0×10^6	36.7	41	0.90	2.76×10^{-5}	236	494
PL–Py	43.4×10^6	73.1	43	1.7	4.38×10^{-5}	942	1939

[a] Determined from the diffusion coefficient at infinite dilution using the Stokes–Einstein equation. [b] Obtained from Zimm plots from SLS. [c] Calculated from $M_{w,app}$ values on the basis of the assumption that PIC micelles were formed at the mixing ratio.

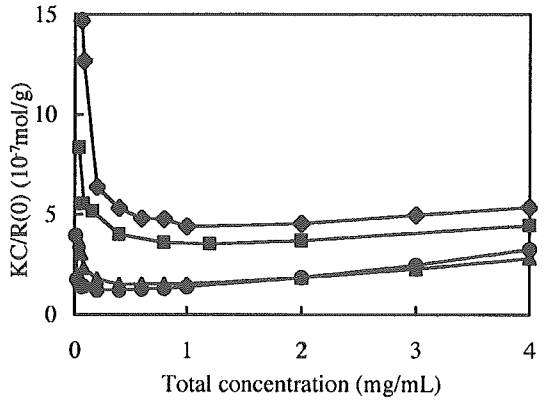

Figure 2. Relationships between the $KC/R(0)$ values obtained from SLS and total concentration of the system (lysozyme + PEG–P(Asp) with or without ω-end-functional groups): detection angles 40, 50, 60, 70, 80, 90, 100, 110, 120, 130, 140 and 150°; temperature = 25 ± 0.2 °C, total concentration = 0.01–5.0 mg/mL; PL micelles (◆), PL–Phe micelles (■), PL–Nap micelles (▲), PL–Py micelles (●).

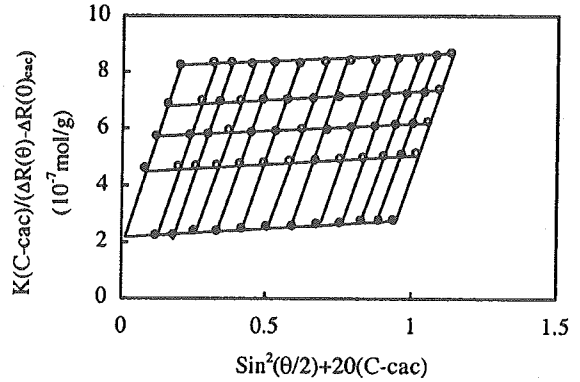

Figure 3. A Zimm plot for PL–Phe micelles: detection angles 40, 50, 60,70, 80, 90, 100, 110, 120, 130, 140, and 150°; total concentration = 2.0, 3.0, 4.0, and 5.0 mg/mL; temperature = 25 ± 0.2 °C.

III. Characterization for PIC Micelles. To gain insight into micellar structure, Zimm plots were made to calculate $M_{w,app}$, R_g, and A_2 for these micelles using the following equation derived from eq 10

$$K(C - \text{cac})/(\Delta R(\theta) - \Delta R(\theta)_{\text{cac}}) = 1/M_{w,app}(1 + q^2R_g^2/3) + 2A_2(C - \text{cac}) \quad (13)$$

As an example, the Zimm plot for PL–Phe micelles is presented in Figure 3. The obtained $M_{w,app}$, R_g, and A_2 values are summarized in Table 2. The hydrodynamic radius (R_h), calculated from the Stokes–Einstein equation (eq 6), and the association number, calculated from the $M_{w,app}$ (calculation method shown in Supporting Information) based on the assumption that PIC micelles had compositions identical to their mixing ratios, are also tabulated in Table 2.

The $M_{w,app}$, R_g, R_h, R_g/R_h, and association number increased in the order: PL < PL–Phe < PL–Nap < PL–Py micelles, consistent with variations observed in cumulant diameters. It appears that increased P(Asp) end-group hydrophobicity promotes aggregation between the block copolymers and the lysozyme. Eventually, an increased association number led to increases in $M_{w,app}$ and R_h. On the other hand, the R_g/R_h values for the PIC micelles are close to 0.776, the theoretical value for a hard sphere,[16] except for the PL–Py micelles with $R_g/R_h = 1.7$ (discussed in the next section). The A_2 values, which reflect interactions between solute and solvent, were quite small and similar (10^{-5} (mol·mL)/g^2) for all PIC micelles with and without hydrophobic groups, suggesting that these terminal hydrophobic groups may be entrapped in the micellar core, and the A_2 values reflect only the interactions between the PEG shell and solvent.

IV. Estimated Micellar Shape. Since theoretical curves of the reciprocal of the particle scattering factor, $P(\theta)^{-1}$ versus $q^2R_g^2$ for various shapes, including a sphere, disk, coil, and rod, are available,[17] micellar shape was estimated directly by comparison of the theoretical curves with those calculated for PIC micelles. Results are shown in Figure 4. The $P(\theta)^{-1}$ values for PL–Nap micelles (▲, Figure 4a) increased with $q^2R_g^2$ along the theoretical curve for a spherical shape, strongly indicating that the PL–Nap micelles may be a spherical particle. For the PL and PL–Phe micelles, the $q^2R_g^2$ values were less than 1.0, below which all the theoretical curves nearly become a single straight line regardless of shape, thus making it difficult to estimate shape for these two micelles from this analysis (data not shown). However, from the dependence of the average characteristic line width ($\bar{\Gamma}$) on the square of the scattering vector (q^2) in Figure 5, all $\bar{\Gamma}$ values for PL, PL–Phe, and PL–Nap micelles could be plotted separately as straight lines with increasing q^2, suggesting that $\bar{\Gamma}/q^2$ (=D) is a constant regardless of the q^2. These results and the PDI values (PDI < 0.1 for PL, PL–Phe, and PL–Nap micelles) support the idea that these three micelle systems may have a spherical shape with an undetectable rotational motion, producing a constant $\bar{\Gamma}/q^2$ value.[18] For the PL–Py micelles (●, Figure 4b), the $P(\theta)^{-1}$ curve plotted against $(qR_g)^2$ was just between the theoretical curves for disk and rod shapes, suggesting that PL–Py micelles deviate from a spherical shape, agreeing well with the high R_g/R_h value for this PL–Py micelle (1.7).

To support these conclusions by another method, radii of the core (r_{core}) for all these micelles as a sphere were separately calculated through the following equation[4b]

$$r_{core} = [(3M_{w,app,core}/4\pi N_A)(W_{P(Asp)}/\sigma_{P(Asp)} + W_{lysozyme}/\sigma_{lysozyme})]^{1/3} \quad (14)$$

where $M_{w,app,core}$ is the weight average molar mass for micellar core obtained from both the molecular weights and association numbers for the P(Asp) and lysozyme, respectively. W_i is the weight fraction, and σ_i are respective densities. The values of $\sigma_{lysozyme}$ ($\sigma_{lysozyme}$ = 1.106 g/cm^3) and $\sigma_{P(Asp)}$ ($\sigma_{P(Asp)}$ = 1.084 g/cm^3) at 25 °C were directly obtained from ref 4b, assuming that the terminal hydrophobic groups and varied Asp unit number elicited

(13) (a) Hnash, C.; Leo, R. L. In *Substituent Constants for Correlation Analysis in Chemistry and Biology*; Wiley: New York, 1979. (b) Guckian, K. M.; Schweitzer, B. A.; Ren, R. X.-F.; Sheils, C. J.; Tahmassebi, D. C.; Kool, E. T. *J. Am. Chem. Soc.* **2000**, *122*, 2213.

(14) Shinoda, K. In *Colloidal Surfactants*; Shinoda, K., Nakagawa, T., Tamanushi, B., Isemura, T., Eds.; Academic Press: New York, 1963; Chapter 1.

(15) Elias, H. G. In *Light Scattering from Polymer Solutions*; Huglin, M. B., Ed.; Academic Press: New York, 1972; Chapter 9.

(16) Douglas, J. F.; Roovers, J.; Freed, K. F. *Macromolecules* **1990**, *23*, 4168.

(17) Geiduschek, E. P.; Holtzer, A. *Adv. Biol. Med. Phys.* **1958**, *6*, 431.

(18) Xu, R.; Winnik, M. A.; Hallett, F. R.; Riess, G.; Croucher, M. D. *Macromolecules* **1991**, *24*, 87.

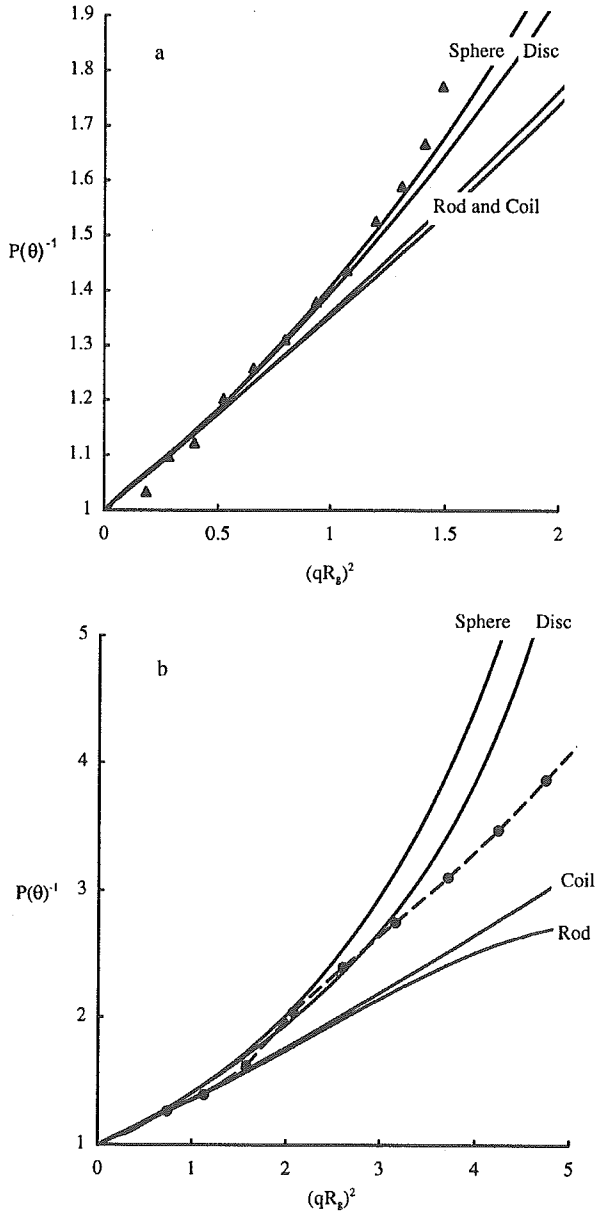

Figure 4. Dependence of $P(\theta)^{-1}$ on $q^2R_g^2$ for PL–Nap micelles (a, ▲) and PL–Py micelles (b, ●). Temperature = 25 ± 0.2 °C.

insignificant variations in the density of the P(Asp) chain. For comparison with the r_{core}, the maximal extension lengths of P(Asp) segments (L_{Asp}) with and without terminal hydrophobic groups were calculated to be 19.3 nm.[19] Here, the contributions for hydrophobic groups were neglected for their smaller size compared with the P(Asp) chain. Table 3 summarizes the r_{core}, L_{Asp}, and r_{core}/L_{Asp} values. Note that only the r_{core}/L_{Asp} value for the PL–Py micelles (1.21) was over 1, inconsistent with a realistic feature that the r_{core} should always be shorter than the L_{Asp}[20] and supporting the conclusion that the PL–Py micelle is not spherical.

It has been asserted previously that both the micellar core and corona contribute to the stabilization and shape transition of block copolymer micelles by using four kinds

(19) Pauling, L.; Corey, R. B. *Proc. Int. Wool Text. Res. Conf.* **1955**, *B*, 249.
(20) Tanford, C. *J. Phys. Chem.* **1974**, *78*, 2469.

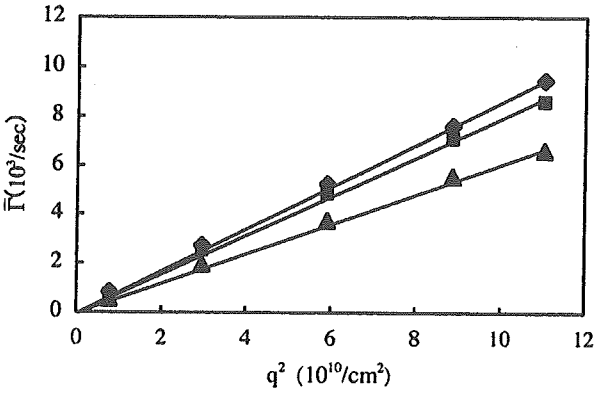

Figure 5. Dependence of $\bar{\Gamma}$ on q^2 obtained from cumulant DLS analysis: PL micelles (◆), PL–Phe micelles (■), PL–Nap micelles (▲); detection angles 30°, 60°, 90°, 120°, and 150°; temperature = 25 ± 0.2 °C, total concentration = 2.0 mg/mL.

Table 3. Calculated Radii of the Core as a Sphere (r_{core}) and Maximal Length of P(Asp) Chain (L_{Asp})

	micelle			
	PL	PL–Phe	PL–Nap	PL–Py
r_{core} (nm)	8.74	10.7	14.0	23.3
L_{Asp} (nm)	19.3	19.3	19.3	19.3
r_{core}/L_{Asp}	0.453	0.554	0.725	1.21

of solvents, in which the core and corona blocks have different solubility. The micellar association number essentially follows the length and solubility of the blocks in the core, and increased association number results in an effective stretching of the inner as well as the corona blocks, the entropy loss of which may induce a sphere–rod transition.[21] In this study, increased association numbers, especially for the PL–Py micelles, were also observed after hydrophobic group introduction. Consequently, the sphere–rod transition for the PL–Py micelles may derive from the stretch of the P(Asp) segments as well as the PEG chains.

V. Micellar Stability versus Ionic Strength Increase. Stability of polyion complexes is strongly affected by medium ionic strength, becoming destabilized with increasing in the ionic strength due to electrostatic shielding effects.[22] To estimate resistance to ionic strength destabilization for PIC micelles, two methods were used. The first compares variations in micellar cac values with increasing NaCl concentrations, based on the prediction that NaCl addition may increase cac values. The second compares observed NaCl-induced variations in micellar light scattering intensity at zero angle (I_{NaCl}) as well as the cumulant diameter. Note that, for sufficient stability against electrostatic shielding effects, a constant I_{NaCl} and cumulant diameter should be observed.

(1) Variations in cac Value. The cac values at various NaCl concentrations (Table 1) were obtained by the same method described in part II. All micellar cac values increased with increasing NaCl concentrations due to weakened core aggregation forces elicited by NaCl electrostatic shielding effects. However, similar to that at NaCl = 0 M, micellar cac values decreased in the order PL > PL–Phe > PL–Nap > PL–Py micelles at identical NaCl concentration, suggesting that micellar stability versus

(21) Antonietti, M.; Heinz, S.; Schmidt, M.; Rosenauer, C. *Macromolecules* **1994**, *27*, 3276.
(22) (a) Abe, K.; Ohno, H.; Tsuchida, E. *Makromol. Chem.* **1977**, *178*, 2285. (b) Tuchida, E.; Osada, Y.; Ohno, H. *J. Macromol. Sci., Part B* **1980**, *17*, 683.

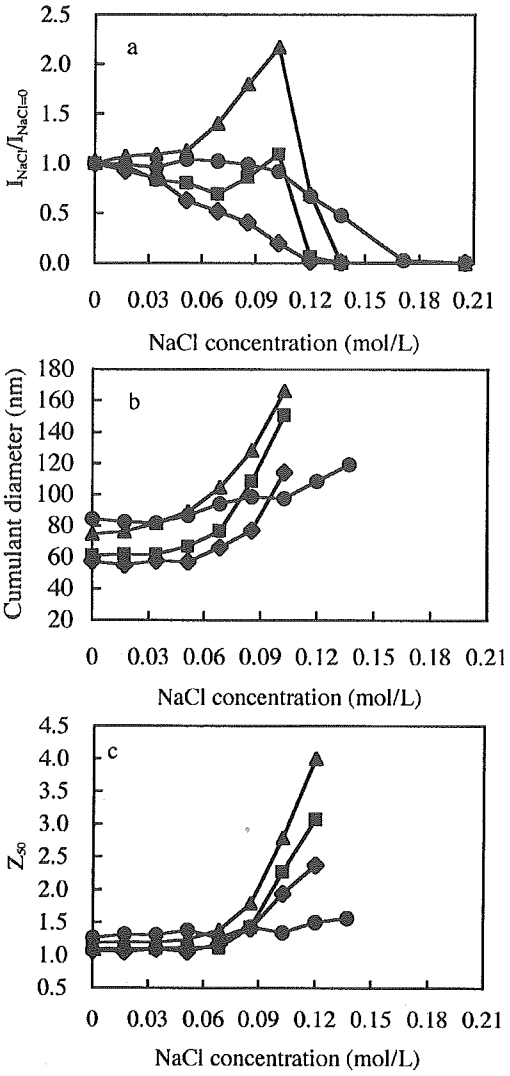

Figure 6. Variations in $I_{NaCl}/I_{NaCl=0}$ (a), cumulant diameter (b), and dissymmetry (c) with increasing NaCl concentrations for PIC micelles. Note that the $I_{NaCl}/I_{NaCl=0}$ values shown at higher salt concentrations were very small but not zero for all the systems. Detection angles were 40, 50, 60, 70, 80, 90, 100, 110, 120, 130, 140, and 150° (a and c) and 90° (b). Total concentration = 2.0 mg/mL, temperature = 25 ± 0.2 °C; PL micelles (◆), PL–Phe micelles (■), PL–Nap micelles (▲), PL-Py micelles (●).

ionic strength increase is significantly enhanced in the opposite order PL < PL–Phe < PL–Nap < PL–Py micelles.

(2) Variations in Light Scattering Intensity. With the purpose of evaluating the variations in micellar I_{NaCl} with increasing NaCl concentrations, ratios of I_{NaCl} to $I_{NaCl=0}$ at NaCl = 0 M ($I_{NaCl}/I_{NaCl=0}$) were employed. As seen in Figure 6a, variations in $I_{NaCl}/I_{NaCl=0}$ for all micelles at 2.0 mg/mL are distinctly different after NaCl addition for 24 h. In the case of PL micelles (◆, Figure 6a), the $I_{NaCl}/I_{NaCl=0}$ monotonically decreased with increasing NaCl concentration, suggesting micellar disintegration. The $I_{NaCl}/I_{NaCl=0}$ for PL–Py micelles (●, Figure 6a) remained almost constant at NaCl < 0.1 M, clearly indicating insignificant variations in I_{NaCl} for this micelle at NaCl < 0.1 M due to sufficient micellar stabilization in this range of ionic strength. However, increased $I_{NaCl}/I_{NaCl=0}$ for PL–Nap micelles (▲, Figure 6a) was obvious with increasing

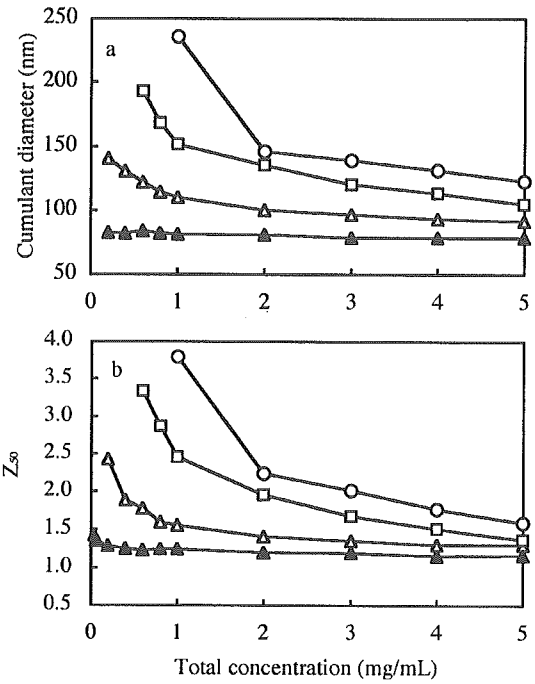

Figure 7. Relationship between cumulant diameter (a) and dissymmetry Z50 (b) with total concentration for PL–Nap micelles at different NaCl concentrations: NaCl = 0 M (▲), 0.05 M (△), 0.08 M (□), 0.09 M (○); temperature = 25 ± 0.1 °C.

NaCl concentrations up to 0.1 M. Similar trends, although slightly moderate, were also observed for the PL–Phe micelle system (■, Figure 6a). Over the same range of NaCl concentrations, both PL–Nap and PL–Phe micelles revealed steep increases in cumulant diameters and dissymmetry, Z_{50} (=I_{50}/I_{130}) (parts b and c of Figure 6), suggesting a probable increase in the association number with a varied micellar shape.[23] It should be noted that a characteristic association with shape variation was reported to occur near cac[24,25] or critical association temperature (cat)[26,27] of polymeric micelles, termed the anomalous micellization phenomenon based on the Aniansson–Wall (A–W) theory.[28] Presumably, with the increased cac value by NaCl additions to 2.0 mg/mL, this type of anomalous micellization may appear for PL–Nap micelles. Indeed, as seen in Figure 7, appreciable increases in the cumulant diameter and Z_{50} for PL–Nap micelles occur in the concentration region near the cac.

On the other hand, for PL–Py micelles, the cumulant diameter (●, Figure 6b) showed only a gradual increase with increasing NaCl concentrations. Dissymmetry values (●, Figure 6c) were also almost constant throughout the entire range of measurement. These results indicate that the shape and size of PL–Py micelles are not sensitive to NaCl at NaCl < 0.1 M, suggesting appreciable stabilization effects of the terminal Py groups in PEG–P(Asp) block copolymer. It has been reported in some papers that there existed specific interactions between Py groups and Trp residues on the surface of lysozyme when pyrene-labeled

(23) Debye, P.; Anacker, E. W. *J. Phys. Colloid Chem.* **1951**, *55*, 644.
(24) Schillen, K.; Brown, W.; Johnsen, R. M. *Macromolecules* **1994**, *27*, 4825.
(25) Molina, L. A.; Freire, J. J. *Macromolecules* **1995**, *28*, 2705.
(26) Iyama, K.; Nose, T. *Polymer* **1998**, *39*, 651.
(27) Tuzer, Z.; Kratochvil, P. In *Surface and Colloid Science*; Matijevic, E., Ed.; Plenum Press: New York, 1993; Vol. 15, p 1.
(28) Aniansson, E. A. G. In *Aggregation Processes in Solution*; Wyn-Jones, E., Gormally, J., Eds.; Elsevier: Amsterdam, 1983; p 70.

polymers associated with lysozyme.[29,30] However, other experiments are necessary to show this for PL−Py micelles.

Conclusions

PIC micelles entrapping lysozyme in their core were prepared through combinations of electrostatic and hydrophobic interactions between this basic enzyme and the PEG−P(Asp) block copolymers bearing hydrophobic groups (Phe, Nap, or Py groups) at the ω-end of the P(Asp) segment. Micelle diameters range from 50 to 90 nm, with unimodal size distributions. Introduction of the Py group produced deviations in micellar shapes from spherical, consistent with an increase in the micellar association number. Both micellar stability against dilution and ionic strength increase were improved by polymer hydrophobic end group introduction. Notably, significantly increased stabilization was achieved for PL−Py micelles, due possibly to any specific interactions between Py groups and Trp residues on the surface of lysozyme.

Acknowledgment. This work was supported by a Grant-in-Aid for Scientific Research from the Ministry of Education, Culture, Sports, Science and Technology (MEXT), Core Research for Evolution of Science and Technology (CREST), Japan Science and Technology Corporation (JST), and 21st century COE program "Human-Friendly Materials based on Chemistry" from MEXT.

Note Added after ASAP Publication. There were errors in the axes of Figures 3 and 5 and footnote *c* of Table 2 and two rows of missing data in Table 3 in the version published ASAP February 12, 2005; the corrected version was published ASAP February 18, 2005.

Supporting Information Available: Calculation of the micellar association number. This material is available free of charge via the Internet at http://pubs.acs.org.

LA0488811

(29) Xia, J.; Dubin, P. L.; Morishima, Y.; Sato, T.; Muhoberac, B. B. *Biopolymers* **1995**, *35*, 411.

(30) (a) Kumar, C. V.; Buranaprapuk, A.; Opiteck, G. J.; Moyer, M. B.; Jockusch, S.; Turro, N, J. *Proc. Natl. Acad. Sci. U.S.A.* **1998**, *95*, 10361. (b) Kumar, C. V.; Buranaprapuk, A. *J. Am. Chem. Soc.* **1999**, *121*, 4262.

Ligand Density Effect on Biorecognition by PEGylated Gold Nanoparticles: Regulated Interaction of RCA_{120} Lectin with Lactose Installed to the Distal End of Tethered PEG Strands on Gold Surface

Seiji Takae,[†] Yoshitsugu Akiyama,[†] Hidenori Otsuka,[‡] Teisaku Nakamura,[†] Yukio Nagasaki,[§] and Kazunori Kataoka*[,†,∥]

Department of Materials Science and Engineering, School of Engineering, The University of Tokyo, 7-3-1 Hongo, Bunkyo-ku, Tokyo 113-8656, Japan, Biomaterials Center, National Institute for Materials Science (NIMS), 1-1 Namiki, Tsukuba, Ibaraki 305-0044, Japan, Tsukuba Research Center for Interdisciplinary Materials Science, Tsukuba University, Tennoudai 1-1-1, Tsukuba 305-8573, Japan, and Center for Disease Biology and Integrative Medicine, School of Medicine, The University of Tokyo, 7-3-1 Hongo, Bunkyo-ku, Tokyo 113-0033, Japan

Received September 14, 2004; Revised Manuscript Received November 17, 2004

PEGylated gold nanoparticles (diameter: 20 nm) possessing various functionalities of lactose ligand on the distal end of tethered PEG ranging from 0 to 65% were prepared to explore the effect of ligand density of the nanoparticles on their lectin binding property. UV−visible spectra of the aqueous solution of the nanoparticles revealed that the strong steric stabilization property of the PEG layer lends the nanoparticles high dispersion stability even under the physiological salt concentration (ionic strength, $I = 0.15$ M). The number of PEG strands on a single particle was determined to be 520 from thermogravimetric analysis (TGA). Scanning electron microscopy (SEM) observation under controlled acceleration voltage revealed the thickness of the PEG layer on the nanoparticle to be ~7 nm. The area occupied by a single lactose molecule on the surface of PEGylated gold nanoparticles was then calculated based on TGA and SEM results and was varied in the range of 10−34 nm^2 depending on the lactose functionality (65~20%). PEGylated gold nanoparticles with 40% and 65% lactose functionality showed a selective and time-dependent aggregation in phosphate buffer with the addition of *Ricinus communis* agglutinin (RCA_{120}) lectin, a bivalent galactose-specific protein. The aggregates can be completely redispersed by adding an excess amount of galactose. Time-lapse monitoring of UV−visible spectra at 600−750 nm revealed that the aggregation of PEGylated gold nanoparticles was accelerated with an increase in both RCA_{120} concentration in the solution and the lactose density of the nanoparticles. Furthermore, the sensitivity of lectin detection could be controlled by the regulation of lactose density on the particle surface. Interestingly, there was a critical lactose density (>20%) observed to induce detectable particle aggregation, indicating that the interaction between the particles is triggered by the multimolecular bridging via lectin molecules.

Introduction

Nanometer-sized metal and semiconductor particles exhibit quantum size effects and have recently attracted growing attention as a simple and sensitive assay method of biologically relevant molecules through the conjugation of ligands on their surface.[1] Particularly, ligand-conjugated gold nanoparticles, an aqueous solution of which is red in color due to the surface plasmon absorption around 520 nm, are useful for the simple and sensitive bioassays[2] because their biospecific aggregation in aqueous medium leads to the formation of a new absorption band at longer wavelength due to the electric dipole−dipole interaction and the coupling between the plasmons of neighboring particles.[3] Nevertheless, the sensitivity of gold nanoparticles as a colloidal sensor system in biological fluids is impaired due to the nonspecific agglomerization particularly at the physiological condition with 0.15 M NaCl as well as to the nonnegligible adsorption of biological components such as proteins and DNA.[4]

Several methods have been applied so far to improve the dispersivity of gold nanoparticles in aqueous medium utilizing surfactants and polymer additives.[5,6] Nevertheless, the long-term stability of the nanoparticles under physiological conditions ($I = 0.15$ M) to avoid nonspecific aggregation has not been well characterized yet. An alternative approach to acquire sterically stabilized gold nanoparticles is, as we reported previously, to modify their surface with end-functionalized and hydrophilic polymer strands such as heterobifunctional poly(ethylene glycol) (PEG) containing both mercapto and acetal terminal groups (acetal-PEG-SH).[7] These α-acetal-PEGylated gold nanoparticles indeed ac-

* To whom correspondence should be addressed. Telephone: +81-3-5841-7138. Fax: +81-3-5841-7139. E-mail: kataoka@bmw.t.u-tokyo.ac.jp.
† School of Engineering, The University of Tokyo.
‡ National Institute for Materials Science (NIMS).
§ Tsukuba University.
∥ School of Medicine, The University of Tokyo.

10.1021/bm049427e CCC: $30.25
Published on Web 01/21/2005

complished a high dispersion stability in physiological conditions. Note that an acetal moiety on the periphery of the PEG brushed-layer can easily be converted under gentle acidic condition into a reactive aldehyde group to conjugate various ligands. As a model ligand, lactose was successfully introduced in the distal end of the PEG chains, inducing selective and reversible aggregation of lactose-functionalized PEGylated gold nanoparticles with a concomitant color change (red−purple−red) by the addition of RCA_{120} lectin.[8]

The molecular recognition process responsible for the aggregation of ligand-installed PEGylated gold nanoparticles is induced through multivalent interaction bridged by the analyte molecules, e.g. lectin. As ligand density is an important factor in this process,[6,8] it is essential to reveal the relationship between the sensitivity of the PEGylated gold nanoparticles and their ligand density for applying them in highly sensitive bioassay. Nevertheless, as far as we know, there is no systematic study on the stringent control of ligand density on gold nanoparticles surfaces to assess the multivalent interaction, which definitely contributes to an increased sensitivity and selectivity because the binding constant based on the multivalent interaction is several orders of magnitude higher than that based on only the monovalent interaction.[9] In this regard, a study reported by Fantuzzi et al. is interesting, revealing that *N*-methylimidazole-fuctionalized gold nanoparticles behave as multivalent ligands for porphyrin arrays with an increase in binding constant of up to 3 orders of magnitude with respect to a monovalent system.[10]

The purpose of the study reported here is to reveal the ligand density effects on the aggregation behavior of ligand-installed PEGylated gold nanoparticles through the evaluation of the interaction between lectin and lactosyl-PEGylated gold nanoparticles with regulated density of lactose. Here, a novel approach is introduced to regulate lactose density on PEGylated gold nanoparticles: Immobilization of the mixtures of oxidized dimers of acetal-PEG-SH and lactosyl-PEG-SH [(acetal-PEG-S-)$_2$ and (lactose-PEG-S-)$_2$, respectively] in various molar ratios. In this way, PEGylated gold nanoparticles with a systematically varying lactose density were prepared to explore the effects of ligand density on the aggregation behavior of gold nanoparticles induced by RCA_{120} lectin.

Experimental Section

Materials. *p*-Aminophenyl β-D-lactopyranoside (Toronto Research Chemicals, Toronto, Canada), sodium cyanoborohydride (Sigma-Aldrich Co., St. Louis, MO), gold colloid (diameter; 20 nm, British Biocell International, Cardiff, U.K.), bovine serum albumin (BSA, Sigma-Aldrich Co., St. Louis, MO), and *Ricinus communis* agglutinin (RCA_{120}, Honen Co., Tokyo, Japan) and the other chemicals were used as received. Water was purified with a Milli-Q instrument (Millipore, Bedford, MA).

Synthesis of (Acetal-PEG-S-)$_2$ and (Lactose-PEG-S-)$_2$. Synthesis of poly(ethylene glycol) derivatives containing both acetal and mercapto terminals (acetal-PEG-SH) was described elsewhere.[7] To obtain the heterobifunctional PEG dimer (acetal-PEG-S-)$_2$, 460 mg of acetal-PEG-SH was

Scheme 1. Synthetic Route of (Lactose-PEG-S-)$_2$

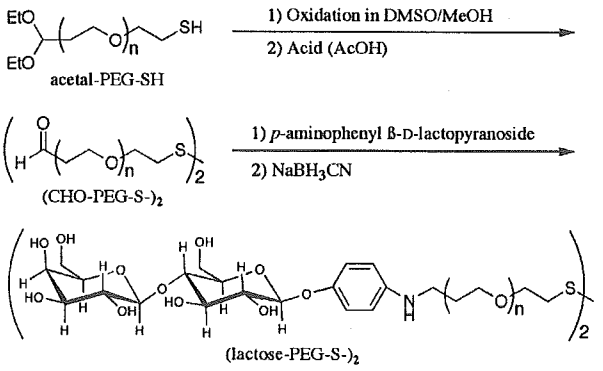

oxidized in 20 mL of DMSO/MeOH (1:1) mixture by stirring 24 h at room temperature in open air condition as shown in Scheme 1. Purification was carried out by dialysis against distilled water and then freeze-dried [yield: 74% (340 mg)]. The successive conversion of acetal groups at the end of (acetal-PEG-S-)$_2$ (50 mg) to the aldehyde group [(CHO−PEG-S-)$_2$] was carried out by the addition of an acetic acid/distilled water (10:1) mixture (3.3 mL). After 5 h stirring at 40 °C, the reaction mixture was added to 30 mL of chloroform followed by washing with 20 mL of saturated NaCl aqueous solution several times. The organic phase was then separated and dried with $MgSO_4$. After the evaporation of the solvent, 30 mL of benzene was added and freeze-dried to obtain the white powder. Then, a 5-fold molar amount of *p*-aminophenyl β-D-lactopyranoside (20 mg) to aldehyde residue in 15 mL of 50 mM phosphate buffered solution (pH = 7.0) was added to the (CHO−PEG-S-)$_2$ in the same flask. After stirring for 15 h at room temperature, 3.0 mg of $NaBH_3CN$ (5-fold molar amount of aldehyde residue in this system) was added to the mixture and stirred for an additional 2 days. Purification was carried out by dialysis against distilled water overnight and then freeze-dried (yield: 78% (39 mg)).

From gel permeation chromatography (GPC), the number-averaged molecular weight (M_n) and the molecular weight distribution (MWD) of (acetal-PEG-S-)$_2$ were determined to be 12 000 and 1.08, respectively, and M_n and MWD of (lactose-PEG-S-)$_2$ were determined to be 12 200 and 1.08, respectively. Lactose conversion ratio was then determined to be 65% from the ^{1}H NMR spectrum (Supporting Information, Figure S1) based on the peak intensity ratio of the phenyl protons of the conjugated *p*-aminophenyl β-D-lactopyranoside (6.5~6.9 ppm) moiety to the methylene protons of PEG chain (3.3~3.8 ppm).

Preparation of PEGylated Gold Nanoparticles Possessing Varying Lactose Functionalities. To obtain PEGylated gold nanoparticles with varying lactose functionalities of 0, 20, 40, and 65% (abbreviated as lac0, lac20, lac40, lac65, respectively), 10 mL of the mixed solution of (acetal-PEG-S-)$_2$ and (lactose-PEG-S-)$_2$ in different molar ratios (total concentration 20 μg/mL) was added to 5 mL of an aqueous dispersion of commercial gold nanoparticles (diameter = 20 nm, 7.0×10^{11} particles/mL) at room temperature. After stirring overnight, to remove excess polymer from the solution, two repeated centrifugation (42 000 × g) and